Brain Structure and Function (2019) 224:2537–2557
https://doi.org/10.1007/s00429-019-01923-8

ORIGINAL ARTICLE

The neglected medial part of macaque area PE: segregated processing of reach depth and direction

Marina De Vitis[1,2,3] · **Rossella Breveglieri**[1] · **Konstantinos Hadjidimitrakis**[1,4,5] · **Wim Vanduffel**[2,3,6,7] · **Claudio Galletti**[1] · **Patrizia Fattori**[1]

Received: 28 March 2019 / Accepted: 13 July 2019 / Published online: 20 July 2019

Abstract

Area PE (Brodmann's area 5), located in the posterior parietal cortex (PPC), is involved in the control of arm movements. Many monkey studies showed PE's involvement in reach directions, while only a few revealed signals coding the depth of reaches. Notably, all these studies focused on the lateral part of PE, leaving its medial part functionally largely unexplored. We here recorded neuronal activity in the medial part of PE in three male *Macaca fascicularis* while they performed coordinated eye and arm movements in darkness towards targets located at different directions and depths. We used the same task as in our previous studies of more caudal PPC sectors (areas V6A and PEc), allowing a direct comparison between these three PPC areas. We found that, in medial PE, reach direction and depth were encoded mainly by distinct populations of neurons. Directional signals were more prominent before movement onset, whereas depth processing occurred mainly during and after movement execution. Visual and somatosensory mapping of medial PE revealed a lack of visual responses yet strong somatosensory sensitivity, with a representation of both upper and lower limbs, distinct from the somatotopy reported in lateral PE. This study shows that PE is strongly involved in motor processing of depth and direction information during reaching. It highlights a trend in medial PPC, going from the joint coding of depth and direction signals caudally, in area V6A, to a largely segregated processing of the two signals rostrally, in area PE.

Keywords Area 5 · Reaching in distance · Arm movements · Superior parietal lobule · Somatosensory responses

Introduction

The posterior parietal cortex (PPC) plays a key role in sensorimotor transformations required to locate targets in 3D space and transforms this spatial information into motor commands to move the hand towards targets in goal-directed actions (Andersen and Cui 2009; Hadjidimitrakis et al. 2012; Andersen et al. 2014). Area PE is part of Brodmann's area 5 (Brodmann 1909), located between Brodmann's areas 2 and PEc in the rostral PPC (Pandya and Seltzer 1982) (Fig. 1). PE receives robust somatic inputs and projections from motor and premotor cortex (Sakata et al. 1973; Jones et al. 1978; Pandya and Seltzer 1982; Johnson et al. 1996; Bakola et al. 2013). Most PE neurons respond to proprioceptive stimulation, with fewer cells sensitive to visual or tactile stimulation (Duffy and Burchfiel 1971; Sakata et al. 1973; Mountcastle et al. 1975; Padberg et al. 2007). The lateral sector of PE contains a rough topographic organization (summarized in Fig. 1a), dominated by the representation of the hand, forelimb, and shoulder

✉ Patrizia Fattori
patrizia.fattori@unibo.it

1 Department of Biomedical and Neuromotor Sciences, University of Bologna, Piazza di Porta S. Donato 2, 40126 Bologna, Italy

2 Laboratory of Neuro- and Psychophysiology, KU Leuven, 3000 Leuven, Belgium

3 Leuven Brain Institute, KU Leuven, 3000 Leuven, Belgium

4 Biomedicine Discovery Institute and Department of Physiology, Monash University, Clayton, VIC 3800, Australia

5 Australian Research Council, Centre of Excellence for Integrative Brain Function, Monash University Node, Clayton, VIC 3800, Australia

6 MGH Martinos Center, Charlestown, MA 02129, USA

7 Harvard Medical School, Boston, MA 02144, USA

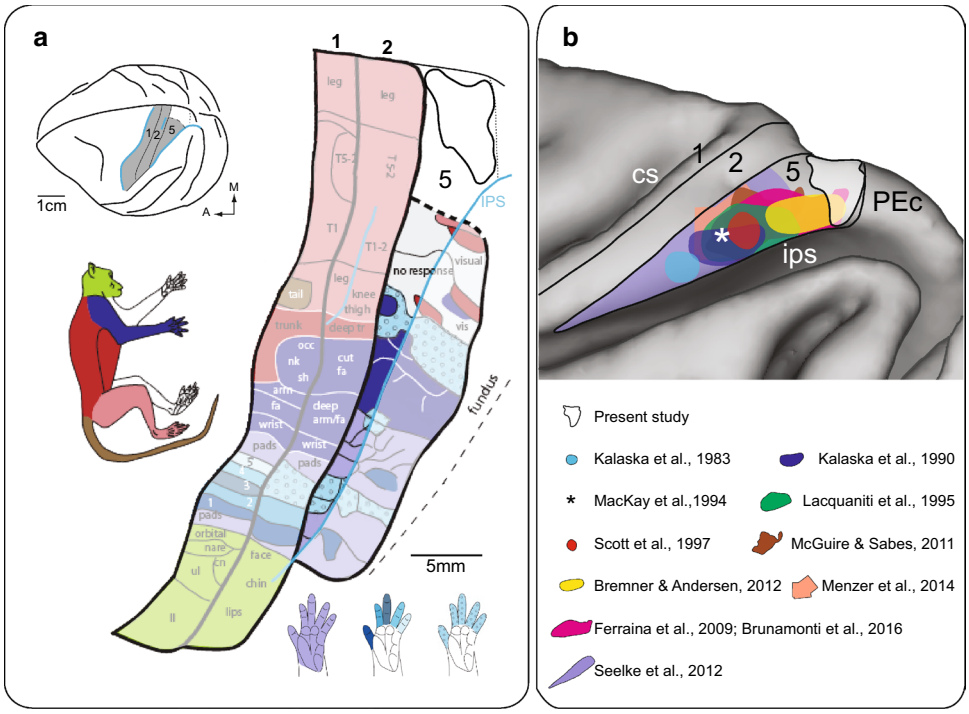

Fig. 1 Recording sites in different PE studies. **a** Cortical representation of somatosensory responses in area PE and indication of the presently recorded part of area PE (white spot with black outline). Top left: dorsolateral view of a macaque brain highlighting in gray the extent of Brodmann's areas 1 and 2 and the explored part of area 5. Right: somatosensory responses recorded from exposed surface of Brodmann's area 5 (bright colors), from nearby areas 1 and 2, and from the medial bank of the intraparietal sulcus (faint colors) (modified from Seelke et al. 2012). Notice that the lateral part of area 5 is dominated by the representations of the digits, hand, and forelimb. The posteromedial part of area 5 has been barely studied. Abbreviations: IPS, intraparietal sulcus; cn, chin; fa, forearm; hl, hindlimb; tr, trunk; occ, occiput; nk, knuckle, sh, shoulder; tr, trunk; ul, upper lip; vis, visual. **b** Enlargement of the superior parietal lobule (SPL) with the location of the parts of area PE previously studied electrophysiologically (colors according to the legend) and of the present study (white spot). Only the papers in which the authors explicitly declared the locations of the penetrations were taken into account for the purpose of reconstructing the recording sites. The tasks used in these studies were: (a) center-out reaches performed with a joystick (Kalaska et al. 1983, 1990; Scott et al. 1997; Menzer et al. 2014), (b) 2D reaches on a touchscreen, either single reaches (Bremner and Andersen 2012), or reaches in a sequence (Mackay et al. 1994) and (c) 3D reaches, either both upward and downward (Lacquaniti et al. 1995), or only upward reaches (Ferraina et al. 2009; Brunamonti et al. 2016), or purely forward reaches at targets located at waist level (McGuire and Sabes 2011). It is worth noting that, until now, reaching and somatosensory studies (**a**) mainly focused on the lateral part of area 5 (PE). Our study is the first investigating the functional properties of the posteromedial part of the area. Abbreviations: cs, central sulcus; IPS, intraparietal sulcus; PEc, area PEc

(Pons et al. 1985; Taoka et al. 1998; Hinkley et al. 2007; Padberg et al. 2007; Seelke et al. 2012), with occasional leg representations. However, the sensory organization of the medial sector of PE is still unknown.

In addition to receiving sensory information, area PE is involved in motor preparation (Burbaud et al. 1991) and in generating body-, shoulder-, or hand-centred coordinates for reaching (Ferraina and Bianchi 1994; Lacquaniti et al. 1995; Kalaska 1996; Ferraina et al. 2009; Bremner and Andersen 2012). PE also sends "command" signals (Mountcastle et al. 1975) directly to spinal cord circuits involved in finger and wrist movements (Rathelot et al. 2017), thereby supporting the earlier view that PE is involved in the coordination of reaching and grasping movements (Gardner et al. 2007; Nelissen and Vanduffel 2011; Gardner 2017; Nelissen et al. 2018).

Most PE studies used center-out reaches without considering reach depth, and reported a high incidence of neurons modulated by arm movement direction (Kalaska et al. 1983, 1985, 1990; Kalaska and Crammond 1992; Ashe and Georgopoulos 1994; Johnson et al. 1996; Kalaska 1996; Scott et al. 1997; Batista et al. 1999; Buneo et al. 2002; Maimon and Assad 2006; Cui and Andersen 2011; Bremner and Andersen 2012; Shi et al. 2013; Li and Cui 2013; Menzer et al. 2014). A few studies have found tuning by reach depth in PE, however, without simultaneously addressing direction processing (Ferraina et al. 2009; Brunamonti et al. 2016). In lateral PE, Lacquaniti et al. (1995) (see Fig. 1b) varied the azimuth, elevation and distance of reach targets with respect to the body and found different neuronal populations processing these parameters. However, in that study, eye position was not monitored, and targets were distributed only between two depth planes.

According to a recent neural tracer study (Padberg et al. 2019), the PE territory is not homogeneous. The medial sector receives stronger afferents from PEc and primary motor cortex (M1) than the lateral sector, and its pattern of connections suggests a more general role in movement coordination (Bakola et al. 2013). In addition, Padberg et al. (2019) found a somatosensory representation of the hand but not of the leg in medial PE. In the present study, we conversely found not only robust arm reach-related activity and somatosensory neurons with receptive fields encompassing the upper limbs, but also a strong lower limb representation. We also studied depth and direction coding of arm reaching movements and examined their time course. Finally, we compared present results with those obtained in the nearby areas V6A and PEc (Hadjidimitrakis et al. 2014a, 2015) to provide a picture of the spatial information processing for reaching in the whole superior parietal lobule (SPL). Our results suggest a substantial degree of functional heterogeneity in the reaching network of SPL and support the view of independent processing of depth and direction information in PE.

Materials and methods

General procedures

Three male macaque monkeys (*Macaca fascicularis*) with a weight ranging between 3.7 and 7.5 kg were involved in the experiments. The study was performed in accordance with the guidelines of EU Directives (86/609/EEC; 2010/63/EU) and Italian national laws (D.L. 116-92, D.L. 26-2014) on the protection of animals used for scientific purposes. Protocols were approved by the Animal Welfare Body of the University of Bologna. During training and recording sessions, particular attention was paid to any behavioral and clinical sign of pain or distress.

Behavioral tasks

Monkeys sat in a primate chair (Crist instruments, Hagerstown, MD, USA) and were trained to perform a Fixation-to-Reach task under controlled conditions to evaluate the effect of depth and direction on reach-related activity of PE cells. Moreover, animals were also trained to perform a Visual fixation task to keep the eyes still during visual stimulations and to stay relaxed during somatosensory stimulations.

Fixation-to-Reach task

This task was performed in darkness with the arm contralateral to the recording hemisphere. During the task, the animals maintained steady fixation on the cued (green) reaching target with their head restrained. Before starting the arm movement, the monkeys kept their hand on a button (home button [HB], 2.5 cm in diameter) located 5 cm in front of the chest on the midsagittal plane (Fig. 2b). Reaches were performed to one of nine light-emitting diodes (LEDs, 6 mm in diameter). The LEDs were mounted on a horizontal panel located in front of the animals, at different distances and directions with respect to the eyes but always at eye level, so the movement performed by the monkeys to reach and press the LED was upward. Target LEDs were arranged in three rows: one central, along the sagittal midline, and two lateral, at version angles of $-15°$ and $+15°$, respectively (Fig. 2c). Along each row, three LEDs were located at vergence angles of 17.1°, 11.4°, and 6.9°. The nearest targets were located at 10 cm from the eyes, whereas the LEDs placed at intermediate and far positions were at a distance of 15 and 25 cm, respectively. The range of vergence angles was selected to include most of the peripersonal space in front of the animals, from very near (10 cm) to the farthest distances reachable by monkeys (25 cm).

The time sequence of the task was identical to the one used in two recent reports involving other SPL areas (Hadjidimitrakis et al. 2014a, 2015, see Fig. 2d). The trial began when the animals pressed the button near their chest, outside the field of view (HB press). After 1 s, one of the nine LEDs was switched on to green (Green-on). The monkeys had to fixate the LED within 500 ms, while keeping the HB button pressed. Then, the monkeys had to wait 1.5–2.5 s for a change in the color of the LED (from green to red) without performing any eye or arm movement. The latter color change was the go signal (Go) for the animals to release the home button and to start an arm movement toward the foveated target (M). Then, the monkeys reached the target (H) and held their hand on the target for 0.8–1.2 s. When the target cue was switched off (Red-off), the monkeys had to release this cue and return to the HB (HB press), which ended the trial and allowed the monkeys to receive a reward. The task was performed in blocks of 90 randomized trials, 10 for each target position. The luminance of LEDs was regulated to compensate for differences in retinal size between LEDs located at different distances. To prevent dark adaptation, the background light was switched on between blocks.

The presentation of stimuli and the animals' performance were automatically controlled and monitored by LabVIEW-based software (National Instruments) as described previously (Kutz et al. 2005), enabling the interruption of the trial if the monkeys broke fixation, made an incorrect arm movement, or did not respect the temporal constraints of the task described above. The correct performance of movements was monitored by pulses from microswitches (monopolar microswitches, RS Components, UK) mounted under the home button and each LED.

At the beginning of each recording session, the monkeys were required to perform a calibration task to calibrate an

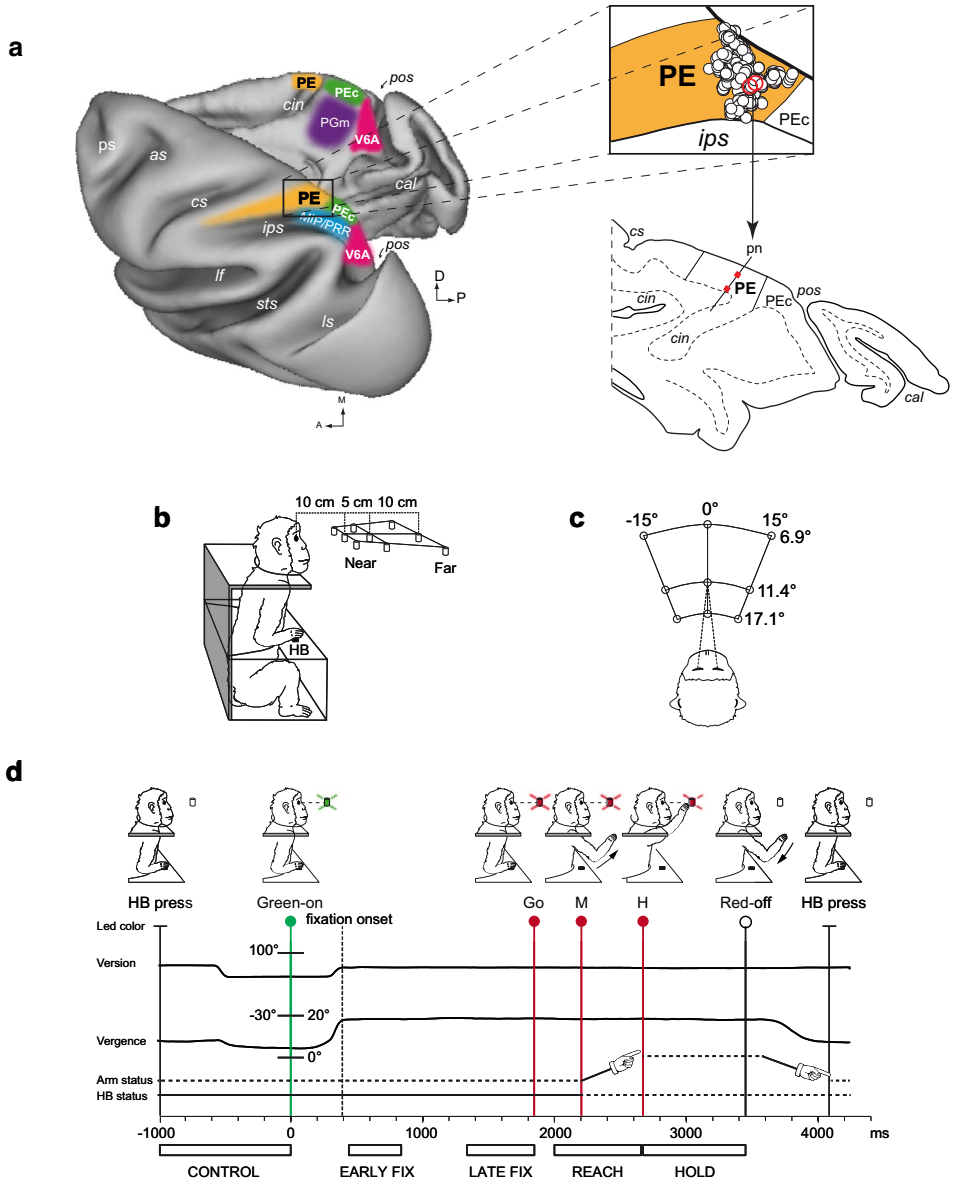

Fig. 2 Reconstruction of our recording site within area PE, experimental set-up and task sequence. **a** Left: Dorsal view of the left hemisphere and a medial view of the right hemisphere of a Macaca fascicularis brain reconstructed in three dimensions using Caret software (http://brainvis.wustl.edu/wiki/index.php/Caret:Download) showing the location and extent of area PE (orange). The other medial PPC areas are also shown: V6A (pink, Galletti et al. 1999); PEc (green, Pandya and Seltzer 1982); medial intraparietal area/parietal reach region (MIP/PRR, light blue; Colby and Duhamel 1991; Snyder et al. 1997); PGm (purple, Pandya and Seltzer 1982). Abbreviations: as, arcuate sulcus; cal, calcarine sulcus; cin, cingulate sulcus; cs, central sulcus; ips, intraparietal sulcus; lf, lateral fissure; ls, lunate sulcus; pos, parieto-occipital sulcus; ps, principal sulcus; sts, superior temporal sulcus; D, dorsal; P, posterior; A, anterior; M, medial. Top right: Enlarged dorsal view of the recorded region, as reconstructed after the histological procedures. Each white dot represents one recorded cell. Bottom right: Parasagittal section of the brain with the reconstruction of a microelectrode penetration ('pn') passing through medial area PE. The red circles indicate recording sites of the cells circled in red in the upper figure. **b** Scheme of the setup used for the Fixation-to-Reach task. Nine light-emitting diodes (LEDs) that were used as fixation and reaching targets were located at eye level. The distances of the 3 targets of the central row from mid-eye level are shown. HB, home button. **c** Top view of the target configuration showing the values of version and vergence angles. **d** Time sequence of task events with LED color, the eye's vergence and version traces, arm status, and HB status. From left to right, vertical lines indicate, respectively, trial start (HB press), target appearance (Green-on), fixation onset (dashed line, end of saccade movement), go signal (Go), start of the arm movement (M), holding phase of the target (H), turning off of the LED (Red-off), and trial end (HB press). The time between the Green-on and the fixation onset was not fixed, as illustrated, but it variated depending on animal's reaction time. Arm drawings indicate the forward and backward arm movement. White bars below the time axis illustrate the time intervals (epochs) used for the analysis of neural activity, from left to right: CONTROL, from home button pressing to fixation LED (Green-on); EARLY FIX, from 50 ms after fixation onset till 450 ms after it; LATE FIX, the last 500 ms before the Go signal; REACH, from 200 ms before the start of the arm movement (M) to the pressing of the LED; HOLD, from LED pressing till the offset of the LED (Red-off)

eye tracker (ISCAN, see below). For the calibration, animals sequentially fixated 5 LEDs mounted on a vertically arranged panel placed at a distance of 15 cm from the eyes. For each eye, we extracted signals for calibration during fixation of five LEDs, arranged in the shape of a cross. One LED was centrally aligned with the eye's straight-ahead position and four LEDs were peripherally placed at an angle of ± 15° (distance: 4 cm) both in the horizontal and vertical axes. From the two individually-calibrated eye position signals, we derived the mean of the two eyes (conjugate or version signal) and the difference between the two eyes (disconjugate or vergence signal) using the following equations:

$$\left[\text{VERSION} = \frac{(R+L)}{2}\right] \,\&\, [\text{VERGENCE} = R - L]$$

where R and L are the gaze direction of the right and left eye, respectively, expressed in degrees of visual angle from the straight-ahead direction.

Visual stimulations

In the Visual fixation task, monkeys were trained to fixate a 0.5° diameter fixation point (FP) on a tangent screen (80° × 80°), 57 cm in front of them, ignoring any other visual stimulus still or moving across the visual field. Monkeys started each trial by pressing the HB and, after 2–6 s the FP turned green. Monkeys had to respond when the FP turned red by releasing the HB in order to receive a reward. The fixation target could appear at different positions on the screen in order to allow visual stimulations even in the far periphery of the visual field. While monkeys were performing the Visual fixation task, individual cells' visual sensitivity was first tested with a series of simple visual stimuli, like light/dark borders, light/dark spots, and bars that were rear-projected on the tangent screen. A cell was considered sensitive to visual stimulations if the discharge, amplified and transformed in audio signals, was higher or lower during stimulations with respect to the baseline discharge, in absence of any other stimulation. If the neuron was unresponsive to these simple visual stimuli, testing was continued using more complex stimuli (light/dark gratings, shadows with irregular contours, shadows rapidly changing in size and/or shape, and corners of different orientation, direction, and speed of movement). If the cell was visually responsive, we mapped the borders of visual receptive field with the stimulus eliciting the best response. Cells responsive to either simple or complex visual stimuli were classified as visual, whereas unresponsive cells were classified as non-visual. A detailed description of the methodology used to test the visual sensitivity in SPL is reported in other papers (Gamberini et al. 2011, 2017).

Passive somatosensory stimulations

Animals got used to be manipulated and touched on the whole body by the experimenter, being rewarded with water and fruits during manipulation. Passive somatosensory stimuli, such as soft manual touching, palpation of deep tissue and joint rotation at different velocities were carried out on the entire body in darkness. Somatosensory stimulation started with superficial tactile stimulation, such as hair bending, superficial touch, or light pressure of the skin. Then we performed deep tactile stimulation (deep pressures of subcutaneous tissues) as well as proprioceptive stimulations (slow and fast rotations of the joints). When a cell responded to joint rotation, we compared neural responses obtained by superficial and deep tactile stimulation of the skin around the joint with those evoked by joint rotation performed without touching the skin around the joint. In some trials, tactile stimulations evoked neural responses that remained constant or were weakened during joint rotation; in others, tactile stimulations were ineffective while joint rotations evoked strong responses. In the first case, the cell was classified as tactile sensitive; in the second, as joint sensitive. In some trials, the cell was responsive to tactile stimulation of the skin around a joint and responded more strongly to joint rotation: these cells were classified as tactile and joint sensitive. We are aware that our operational criteria do not exclude the possible participation of other somatosensory afferences, including muscle proprioception, and that neck rotation could not be tested in our experimental conditions because the experiments were performed with the monkey's head fixed. The same procedure has been used by our lab in other SPL areas (Breveglieri et al. 2002, 2006, 2008; Gamberini et al. 2017).

In both Visual fixation task and somatosensory stimulations, eye position was monitored to exclude the possibility that observed neuronal modulations were due to oculomotor activity. If the neural discharge was influenced by eye movements, visual/somatosensory stimulations were repeated until neural activity was collected under stable fixation behavior.

Surgical and recording procedures

A head-fixation system and a recording chamber were surgically implanted using aseptic procedures and under general anesthesia (sodium thiopenthal, 8 mg/kg/h, *i.v.*) following the procedures reported in Galletti et al. (1995). A full program of postoperative analgesia (ketorolac trometazyn, 1 mg/kg, *i.m.,* immediately after surgery, and 1.6 mg/kg, *i.m.*, on the following days) and antibiotic care [Ritardomicina® (benzathine benzylpenicillin + dihydrostreptomycin + streptomycin) 1–1.5 ml/10 kg every 5–6 days] followed the surgery.

Extracellular recording techniques and procedures to reconstruct microelectrode penetrations were similar to those described in other studies (Galletti et al. 1996; Breveglieri et al. 2006, 2014; Gamberini et al. 2011, 2017). Single-cell activity was extracellularly recorded from area PE, located mainly on the exposed cortex of the postcentral gyrus, between somatosensory cortex and PEc (Fig. 2a) (Pandya and Seltzer 1982). We performed single microelectrode penetrations from the posteromedial part of PE, using multielectrode recording systems (5-channel MiniMatrix, Thomas Recording, GMbH, Giessen, Germany, for 2 animals, and 4-channels Alpha Omega Tower, Alpha Omega Engineering, Nazareth, Israel, for 1 animal). The electrode signals were amplified (at a gain of 10,000) and bandpass filtered (between 0.5 and 5 kHz). Action potentials in each channel were isolated online with a waveform discriminator (Multi Spike Detector; Alpha Omega Engineering, Nazareth, Israel, sampling rate 60 kHz). Eye position signals were sampled with 2 cameras (one for each eye) at 100 Hz and were controlled by a virtual window (4 × 4 degrees) centered on the fixation target. If monkeys fixated outside this window, the trial was aborted.

Histological reconstruction of electrode penetrations was performed following the procedures detailed in studies from our lab (Gamberini et al. 2011, 2017). Briefly, electrode tracks and the approximate location of each recording site were reconstructed on histological sections of the brain on the basis of electrolytic lesions and the coordinates of penetrations within the recording chamber. Present work includes only the neurons assigned to area PE following the cytoarchitectonic criteria according to Pandya and Seltzer (1982). The recording site involved the medial part of area PE (Fig. 2a).

Data analysis

All the analyses were performed using custom scripts in Matlab (Mathworks, Natick, MA, US, RRID: SCR_001622) and STATISTICA software (StatSoft, Tulsa, OK, US, RRID: SCR_014213). Most of these analyses have been performed also in two recent papers from our lab (Hadjidimitrakis et al. 2014a, 2015), which allows direct comparisons among the three SPL areas: PE, PEc, and V6A.

Analysis of the neuronal activity during the Fixation-to-Reach task was made by quantifying the discharge recorded during each trial in the following time epochs:

- CONTROL, from HB pressing to fixation LED lighting up. It contains the neural discharge before fixation onset. This epoch has been only used to calculate the latency of the reach-related responses (see following "Materials and methods");
- EARLY FIX, from 50 ms after the end of the saccade to the green LED till 450 ms afterwards. It contains the neural discharge for LED fixation;
- LATE FIX, the last 500 ms before the go-signal. It contains the cells' discharge during arm movement preparation;
- REACH, from 200 ms before arm movement onset (HB release) until the red target LED was reached. It contains the discharge of the cells during reaching execution. From trial to trial, this epoch was of different duration, depending on animal's movement times;
- HOLD, from LED pressing till the target (red LED) offset. It contains the discharge of the cells during LED pressing.

Movement times in reaching trials were calculated as the time difference between HB release and target LED press, as detected by presses/releases of the microswitches.

The effect of target depth and direction on neural activity was analyzed only for those units with a mean firing rate higher than 3 spikes/s in at least one spatial position. In addition, we only included those neurons that were recorded during at least 7 trials per spatial position. The reasons for these conservative criteria are dictated by the intrinsic high variability of biological responses, particularly in the PPC, and are explained in detail in Kutz et al. (2003).

We first used a 2-way analysis of variance (ANOVA) to quantify the proportion of neurons modulated by each variable in each epoch. Target depth was defined as the distance of the target from the animal (near, intermediate, far), and target direction as its position with respect to the recording hemisphere (ipsilateral, central, contralateral). We considered that neurons were modulated by a given factor only when the factor's main effect was significant ($p < 0.05$). Given that the target was foveated in all epochs of interest, its depth and direction in space were determined by the vergence and version angles of the eyes, respectively. That said, when we refer to spatial tuning analysis and data in the remainder of this article, the terms depth and vergence, as well as direction and version, are interchangeable.

We applied a two-proportion z-test (Zar 1999), as detailed in Fluet et al. (2010), to make comparisons between the proportion of cells modulated by depth, direction or both. To perform this test, the SE of the sampling distribution difference between two proportions was computed as:

$$SE = \sqrt{p(1-p)[(1 \div n_1)(1 \div n_2)]}$$

with $p = [(n_1 \times p_1)(n_2 \times p_2)] \div (n_1 + n_2)$ representing the pooled sample proportion and n_1/p_1 and n_2/p_2 representing the size and proportion, respectively, of each sample. Subsequently, the z score was calculated as $z = (p_1 - p_2)/SE$, and its corresponding P value was obtained from the (cumulative) normal distribution.

To investigate the population activity during the course of a trial, we tested for significant tuning at multiple time points t using a 2-way ANOVA on the spike count in a 200 ms window centered around t. This test was repeated in time steps of 50 ms (sliding window ANOVA, $p<0.05$, Fig. 4b). Criteria for significant tuning were the same as for the ANOVA analysis of the fixed time epochs.

To analyze the spatial tuning of activity, a stepwise multiple linear regression model was applied in each epoch of interest. To relate the neural activity in the epochs of interest to the different target positions, we applied the following equation for the firing rate using this regression model:

$$A\left(X_i, Y_i\right) = b_0 + b_1 X_i + b_2 Y_i$$

where A was the neural activity in spikes per second for the ith trials; X_i and Y_i the positions of the target defined as vergence and version angles, respectively, of the eyes; b_1 and b_2 were regression coefficients and b_0 the intercept. After being tested for their significance, the vergence and version coefficients were normalized with the standard deviation of vergence and version, correspondingly. The normalized coefficients allow a comparison among the independent variables and provide information about their relative influence in the regression equation. In the present study, this allowed us to compare the vergence and version coefficients and to account for differences in range of angles for vergence and version (10.2° vs. 30°, respectively). The regression coefficients were selected using a backward stepwise algorithm (Matlab function "stepwise") that determined whether the coefficients were significantly different from zero. At the end of the stepwise algorithm, only the coefficients that were statistically different from zero remained ($p<0.05$). These coefficients were then used to determine the spatial preference only in the cells with a significant main effect (ANOVA, $p<0.05$) in a certain epoch. In each neuron, the sign of the linear correlation coefficients (normalized) were used to determine the spatial preference in a certain epoch. In those cases in which the linear coefficients were not significant, but the neurons were modulated by at least one of the two factors considered in the ANOVA (i.e. depth and direction), a Bonferroni post hoc test ($p<0.05$) was applied to define the preferred position.

To quantify the spatial selectivity of neurons linearly modulated by depth or direction, we calculated selectivity indices (SI) which take into account the magnitude of the neurons' response to the movement depth and direction evoking the highest discharge. We calculated the SI separately for depth and direction using the following equations:

$$\left[\mathrm{SI}_{\mathrm{depth}} = \frac{(\text{best far} - \text{best near})}{(\text{best far} + \text{best near})}\right] \;\&\; \left[\mathrm{SI}_{\mathrm{direction}} = \frac{(\text{best contra} - \text{best ipsi})}{(\text{best contra} + \text{best ipsi})}\right]$$

where 'best far' and 'best near' are the activities for the far and near positions, respectively, evoking the highest discharge, and 'best contra' and 'best ipsi' are the activities for the contralateral and ipsilateral positions, respectively, evoking the highest discharge. The indices range from −1 to 1. Neurons with values close to −1 indicate a high selectivity for NEAR (or IPSILATERAL) positions, whereas values close to 1 denotes neurons with a high selectivity for FAR (or CONTRALATERAL) positions in 3D space. Values close to 0 indicate a similar response for all reach depths (or directions). We used a two-sample Kolmogorov–Smirnov test to compare the cumulative distributions of $\mathrm{SI}_{\mathrm{depth}}$ and $\mathrm{SI}_{\mathrm{direction}}$ in each epoch ($p<0.01$).

Population responses of neurons modulated by target depth/direction in the epochs of interest were computed as averaged spike density functions (SDFs). For each neuron, an SDF was calculated (Gaussian kernel, half-width at half maximum 40 ms) for each trial and averaged across all the trials of the preferred and non-preferred depths and directions as defined by the linear regression analysis. We found the peak discharge rate of the preferred condition and used it to normalize the SDF. Population SDF curves representing the activity of the preferred and non-preferred target positions were constructed by averaging the individually-normalized SDFs of the cells (Marzocchi et al. 2008), aligned at the behavioral event of interest. We statistically compared the population SDFs curves of preferred and non-preferred positions with a permutation test (10,000 iterations) comparing the sum of squared errors of the actual and randomly permuted data. The intervals of the curve that we compared were different according to the epoch considered: for cells modulated by depth/direction during EARLY FIX, the interval was from 50 to 450 ms after saccade offset; for cells modulated during REACH, the interval was from 200 ms before the movement onset until the red target LED was reached.

To find the onset of the reach-related response, a sliding window (width = 20 ms, shifted by 2 ms) was used to measure the activity starting from 200 ms before the movement onset in all of the tested conditions. This activity was compared with the firing rate observed in the 1000 ms before fixation LED onset (CONTROL epoch, Student's t test, $p<0.05$) in agreement with what was used in another PE study (Kalaska et al. 1983). The onset of the response was determined as the time of the first of 5 consecutive bins (10 ms), where comparisons were statistically significant ($p<0.05$). The above procedure, also used in a recent V6A paper (Hadjidimitrakis et al. 2014a), was adapted from earlier work (Nakamura and Colby 2000).

Results

In the present study, we investigated the functional properties of the medial part of PE (see Fig. 1), a cortical area largely neglected in previous studies. We evaluated the influence of depth and direction of reaching on the activity of PE cells during reaches in 3D space. We used a Fixation-to-Reach task whereby target elevation was kept constant at eye level (Fig. 2b), to avoid the possible modulating effect of gaze elevation on cell discharge, a factor effectively modulating many PPC cells (see Galletti et al. 1995; Hadjidimitrakis et al. 2011). This task required the monkeys to transport the hand from a fixed position near the body to one of nine targets in peripersonal space.

We recorded activity of 176 single PE neurons in five hemispheres of three monkeys (left hemisphere/total: M1, 24/90; M2, 51/73; M3, 13/13). No significant differences between results from different monkeys were found in all the analyses performed (Chi squared test, $p > 0.05$), thus they will be presented jointly. The histological reconstruction of recording sites showed that microelectrode penetrations were performed in the medial part of area PE (see inset in Fig. 2a). We examined the neural responses during four epoch intervals: initial LED fixation (EARLY FIX, see "Materials and methods"), movement preparation (LATE FIX), movement execution (REACH), and LED holding (HOLD).

Figure 3 shows two examples of the most represented classes of PE cells: those tuned only by depth (Fig. 3a, 2-way ANOVA, $p < 0.0001$ in EARLY FIX, $p < 10^{-9}$ in LATE FIX, $p < 10^{-27}$ in REACH, $p < 10^{-26}$ in HOLD) and those tuned only by direction (Fig. 3b, 2-way ANOVA, $p < 10^{-5}$ in LATE FIX, $p < 0.01$ in REACH, $p < 10^{-10}$ in HOLD). The neuron in Fig. 3a increased its discharge rate right before the movement onset (mean reach-related incremental response relative to HB release: -120 ± 83 ms, SD) and peaked in activity during the arm movement. The cell exhibited a preference for near and intermediate space (Fig. 3a, bottom and intermediate rows) during all the epochs considered, particularly during the execution of reaching movement and LED pressing (epochs REACH (R) and HOLD (H) in Fig. 3a). The neuron in Fig. 3b discharged strongly during the execution of reaches and LED pressing for ipsilateral and central positions with respect to the recording hemisphere (Fig. 3b, left and central columns). Contrary to the previous example, the discharge rate increased after the arm movement onset (reach-related incremental response: $+102 \pm 93$ ms, SD) and was maintained during the HOLD epoch.

The neuron of Fig. 3a showed also a weak tuning of activity and slightly increased its discharge rate during the EARLY FIX and LATE FIX epochs (Fig. 3a, EF and LF respectively). As in the reaching and holding epochs, the activity was higher during EARLY FIX and LATE FIX for the nearest positions. The neuron of Fig. 3b reduced its activity during the last part of EARLY FIX and throughout the LATE FIX part of the trial (Fig. 3b, EF and LF respectively). This inhibition of activity during LATE FIX was spatially tuned, with stronger effects for the ipsilateral and near space.

Dynamic depth and direction tuning during the task

Modulation of neural activity by depth and direction was studied through a two-way ANOVA ($p < 0.05$) with target depth (near, intermediate, far with respect to the body) and target direction (contralateral, center, ipsilateral with respect to the recording hemisphere) being the two factors in each task epoch. One hundred thirty-nine PE neurons (79%) were modulated by at least one of the two factors in at least one epoch. Interaction effects between the 2 factors was observed in 6% of the cells across epochs. However, very few neurons (3%) showed *only* the interaction effect, so hereafter only the main effects of depth and direction will be considered. The results of the two-way ANOVA for each epoch are reported in Fig. 4a. Neurons modulated only by depth or only by direction were the most represented classes of tuned cells in area PE (see Fig. 4a, DEPTH and DIRECTION respectively). The incidence of neurons modulated only by depth or direction followed a different time course across epochs. The percentage of depth modulated neurons significantly increased (two proportion *z*-test, EARLY FIX vs. REACH, $p = 0.008$) from 14% and 12% (EARLY FIX and LATE FIX, respectively) before the arm movement to 24% and 22% during REACH and HOLD. By contrast, the direction-modulated neurons peaked during the fixation epoch (EARLY FIX, 18%), significantly decreased during the LATE FIX and REACH (12 and 10% respectively, two proportion z-test, EARLY FIX vs. REACH, $p = 0.015$) and slightly increased again during HOLD (15%). Across epochs only about 10% of cells was modulated by both signals ('BOTH', Fig. 4a), with a mild though insignificant increase in selectivity during the last phases of the task (two proportion z-test, EARLY FIX vs. HOLD, $p = 0.07$). The low proportion of 'BOTH' cells suggests a substantial degree of separation between depth and direction signals, especially during REACH and HOLD, where the fraction of depth-modulated cells ('DEPTH') was significantly different from 'BOTH' cells (two-proportion z-test, $p = 0.0006$ in REACH, $p = 0.02$ in HOLD). We also tested whether the proportion of cells tuned for both depth and direction differ significantly from chance level, given the percentages of depth and directionally modulated cells. We found that the percentages of 'BOTH' cells did not differ significantly from chance in any of the tested epochs (two-proportion z-test, $p > 0.05$).

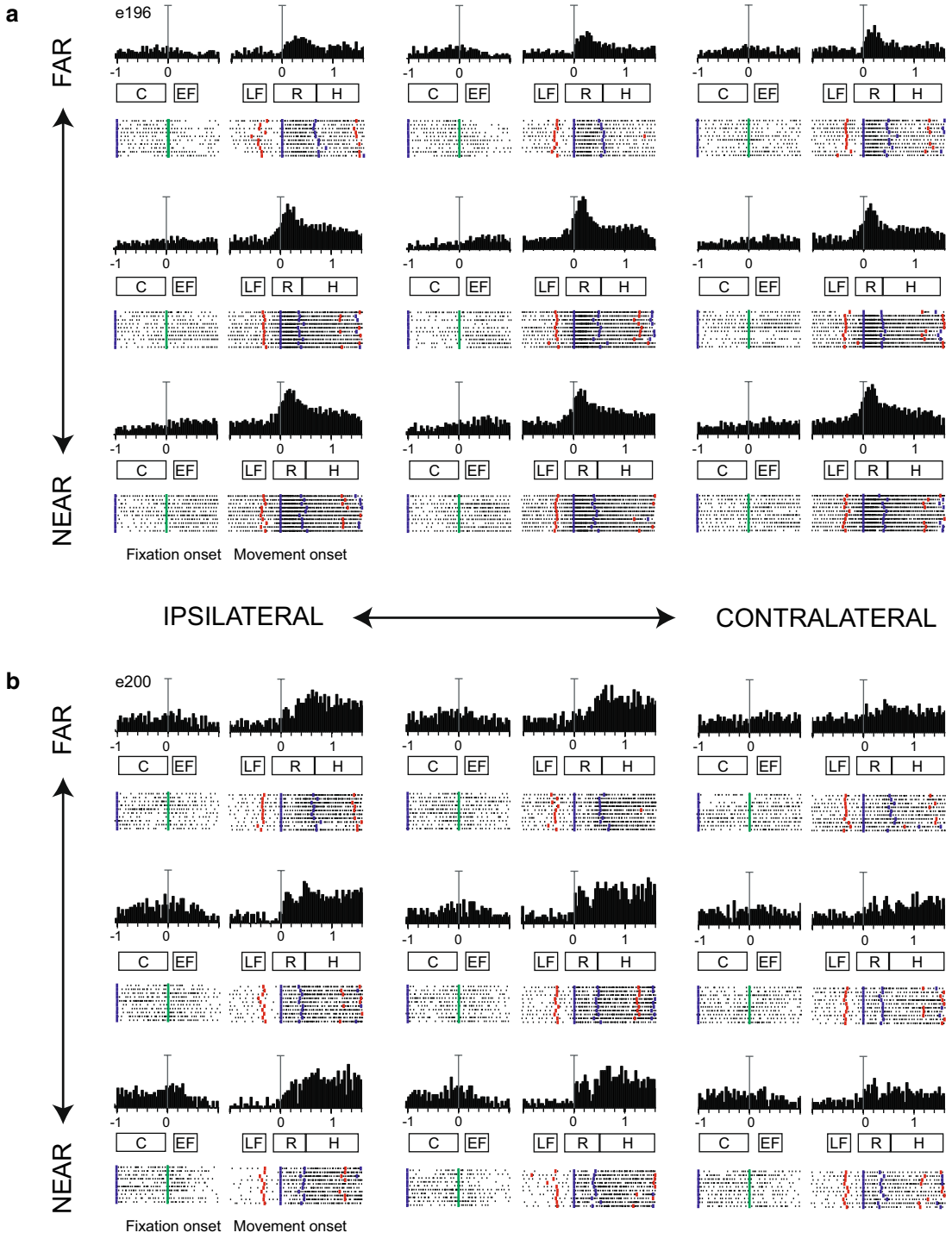

Fig. 3 Examples of medial PE neurons modulated by depth **(a)** and direction **(b)**. **a** Neuron showing depth tuning starting immediately before movement onset and reaching its maximum during movement execution. Spike histograms (top), and rasters (middle), are shown for the 9 target positions. Coloured behavioral markers are from left to right: HB pressing, fixation onset, go signal, movement onset, movement end, target offset, backward movement onset. Rows represent the 3 depths (from bottom to top: NEAR, INTERMEDIATE, FAR) and columns the 3 directions (from left to right: IPSILATERAL, CENTRAL, CONTRALATERAL). Activities are aligned to fixation onset and arm movement onset. Horizontal scale: 200 ms/div. Vertical scale bar on histogram: 90 spikes/s. Rectangles below histograms indicate the duration of the epochs CONTROL (C), EARLY FIX (EF), LATE FIX (LF), REACH (R), HOLD (H). **b** Neuron showing a preference for ipsilateral space during reaching execution and holding time. All conventions are as in **(a)**, vertical scale on histogram: 73 spikes/s

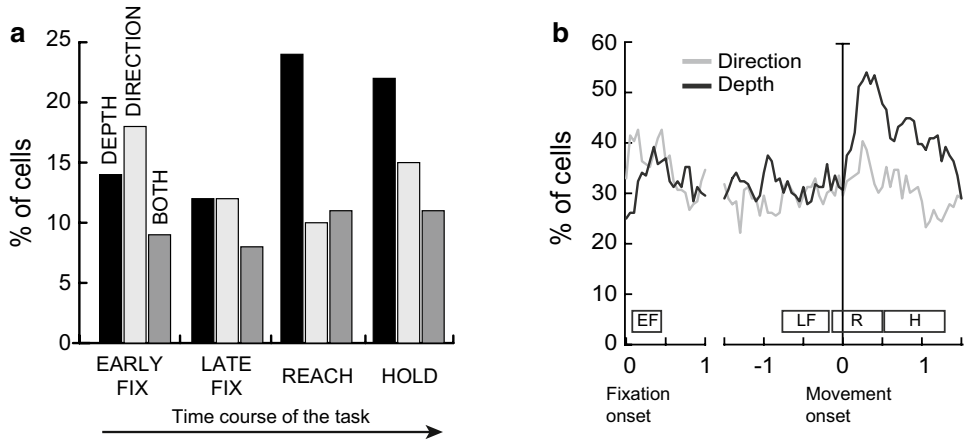

Fig. 4 Distribution of the incidence of significant effects modulating PE cells and strength of depth and directional tuning. **a** Histograms show the results of a two-way ANOVA (factors: DEPTH and DIRECTION, $p<0.05$) as incidence of modulated cells during the target fixation (epoch EARLY FIX), reaching preparation (epoch LATE FIX), execution (epoch REACH) and LED pressing (epoch HOLD). **b** Percentage of tuned cells by depth (black line) and direction (gray line) in a sliding window ANOVA (width: 200 ms, step: 50 ms). Trials are aligned to fixation and movement onsets. Rectangles below each plot indicate the functional time epochs ('EF', EARLY FIX; 'LF', LATE FIX; 'R', REACH; 'H', HOLD)

Table 1 Number of neurons modulated by depth and direction in each epoch

	Depth		Direction	
	ANOVA	Regression	ANOVA	Regression
Early fix	40/176 (23%)	30/40 (75%)	47/176 (27%)	35/47 (74%)
Late fix	35/176 (20%)	26/35 (74%)	35/176 (20%)	25/35 (71%)
Reach	62/176 (35%)	52/62 (84%)	36/176 (20%)	30/36 (83%)
Hold	57/176 (32%)	51/57 (89%)	45/176 (26%)	35/45 (78%)

To examine the temporal evolution of tuning with finer detail we performed a sliding window analysis (Fig. 4b; width: 200 ms, step: 50 ms) that confirmed the time course of the modulating effects suggested by the plot in Fig. 4a: the percentage of cells modulated by depth (Fig. 4b, black line) surpassed those modulated by direction (Fig. 4b, gray line) immediately after movement onset, and this effect was maintained during the HOLD epoch (see Fig. 4b).

Space representations across different epochs

To characterize the spatial preference of modulated neurons, a linear regression analysis was performed, considering target depth and direction as independent variables. We decided to apply this model because we observed that the modulations were generally of planar type and only a few neurons gave their maximum response for central positions (3% of cells, Bonferroni post hoc test). We calculated the percentage of neurons modulated by target depth and direction (two-way ANOVA, $p<0.05$) with a significant linear correlation ($p<0.05$). As shown in Table 1, the number of PE neurons modulated by depth with significant linear regression coefficients slightly increased across the task epochs, and a similar trend was observed for neurons modulated by direction.

Neurons modulated by depth were classified as 'NEAR' or 'FAR' and neurons with directional tuning as 'CONTRALATERAL' or 'IPSILATERAL', depending on the sign of the correlation coefficient. Figure 5a shows that the majority of cells modulated only by depth (Fig. 5a, top panels) preferred far spatial positions in all epochs, though this preference was significant only during the REACH epoch (Chi squared test, $p<0.01$). This bias for far spatial positions most likely reflects a movement amplitude, and this is corroborated by the fact that all animals showed longer arm movement durations when targets were located in the far space [mean movement time for near space: 546 ± 53 ms, SD; mean movement time for far space: 631 ± 64 ms, SD (ANOVA, $p=4*10^{-34}$)]. Cells tuned only for direction (Fig. 5a, bottom panels) showed a gradual shift from a slight preference for the CONTRALATERAL space in 'EARLY FIX' to a more pronounced preference for the IPSILATERAL space in 'HOLD', achieving statistical significance only in this latter epoch (Chi squared test, $p<0.05$).

To quantify the strength of the spatial tuning, we calculated a selectivity index for each modulated neuron, disjointly for depth and direction (SI; see "Materials and methods"). The value of SI, which ranges from −1 to 1, indicates whether neurons discharged more for FAR versus NEAR, or CONTRALATERAL vs. IPSILATERAL positions. The SI distributions are shown in Fig. 5b, separately for each action epoch. The analysis shows a significant difference between the distributions of SI_{depth} and $SI_{direction}$ during the REACH and HOLD epochs (two-samples Kolmogorov–Smirnov test,

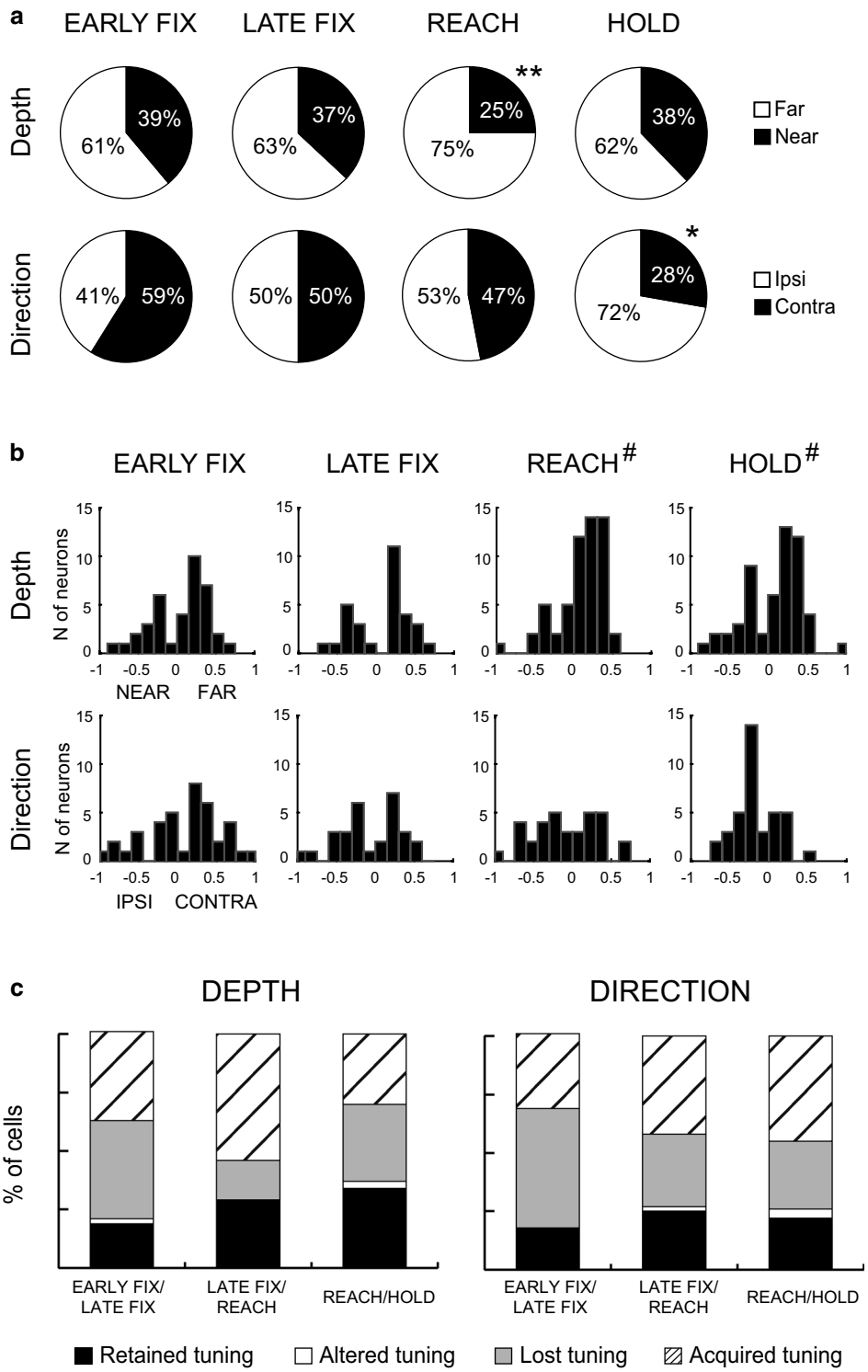

Fig. 5 Spatial preference, indices and tuning consistency across different epochs. **a** Top: Percentage of cells modulated by depth with a preference for far ('FAR', white) or near ('NEAR', black) space in each epoch. Bottom: Percentage of the cells linearly modulated by direction with a preference for ipsilateral ('IPSI', white) or contralateral ('CONTRA', black) space in each epoch. Asterisks indicate a statistically significant spatial preference (*: Chi squared test, $p < 0.05$, **: Chi squared test, $p < 0.01$. The Chi squared test was performed on the numbers of neurons in each of the compared group). **b** Distribution of selectivity indices of reaching cells calculated for EARLY FIX, LATE FIX, REACH, and HOLD for depth and direction separately. Data refer to reach-related activity collected while the animal performed an arm movement directed toward the preferred spatial position. Negative values of the index indicate neurons that present stronger selectivity for 'NEAR' and 'IPSI' positions; positive values neurons that show higher selectivity for 'FAR' and 'CONTRA' positions. Hashes indicate a statistical difference between the cumulative distributions of SI_{depth} and $SI_{direction}$ (two-samples Kolmogorov–Smirnov test, $p < 0.01$). **c** Percentages of cells that retained (black), altered (white), lost (light gray) or acquired later (hatched) their tuning in depth (left) and direction (right) in pairs of consecutive epochs during the task

$p < 0.01$), with neural discharges more selective for farthest and ipsilateral targets. To evaluate the consistency of spatial preference across single neurons, we quantified the cells that retained, altered, lost, or acquired their spatial preference from one epoch to the next. As shown in Fig. 5c, the incidence of cells that retained their spatial preference is quite low (about 25%), both in depth and in direction. Many cells acquired or lost their tuning during the time-course of the trial, both in depth and in direction. This was particularly evident at the transition from the LATE FIX to the REACH epoch, with more than half of the cells (54%) becoming depth tuned at the later epoch. The same trend was evident

in the cells tuned for direction (Fig. 5c, right), where a considerable number of neurons lost their spatial tuning after the early phases of the task (EARLY FIX/LATE FIX, 51%), and an increasing number of cells acquired their spatial tuning as the task progressed (LATE FIX/REACH, REACH/HOLD, 30%). In summary, the trends were similar for depth and direction, with a remarkable increase in the number of spatially tuned cells -especially for depth-tuned cells- as the trial progresses from action preparation to execution.

Cell categories

Changes in neuronal tuning from epoch to epoch formed the basis of a complementary system of cell classification. To this regard, PE cells could be divided in three categories: "*Fix*" neurons, that showed a significant change in activity at the onset of fixation (EARLY FIX) and a spatial tuning during EARLY FIX, but not during REACH; "*Reach*" neurons, showing the opposite modulation; "*Fix-Reach*" neurons, responsive and spatially tuned in both epochs. We adopted the same categorization scheme already used in our studies of V6A and PEc (Hadjidimitrakis et al. 2014a, 2015), and this enabled us to make comparisons of PE categories with the same categories in V6A and PEc (see below). Moreover, the vast majority of PE cells modulated before the movement onset (epoch LATE FIX) belonged to one of the categories mentioned above (~ 75% of depth modulated cells, ~ 60% of directional modulated cells, 2-way ANOVA, $p < 0.05$). Figure 6a shows that the three cell categories (Fix, Reach, Fix-Reach) were differently represented (Chi squared test, $p < 0.01$) between depth- and direction-modulated cells. The largest fraction of neurons modulated by depth were REACH cells (32%, $N = 44/139$), with the other categories containing half or less cells (Fig. 6a left, 16% Fix, 13% Fix-Reach, Chi squared test, $p < 0.05$). In contrast, neurons affected by direction were virtually equally distributed among the three classes (Fig. 6a, right; Chi squared test, $p > 0.05$). Figure 6b shows the anatomical distribution of the three types of cells in the part of area PE we studied. Each circle represents one cell. There was no obvious spatial clustering or gradient between the three cell categories that was sufficiently regular across the five hemispheres studied.

To evaluate the tuning of Fix, Reach, and Fix-Reach cells at population level, we calculated the average normalized spike density functions (SDFs), separately for the three different cell categories. Figure 6c illustrates the average population activity of each category of cells for depth-modulated (left panels) and direction-modulated (right panels) cells. As expected, the activity in the preferred and non-preferred conditions of Fix cells (Fig. 6c, top panels) started to diverge immediately after the onset of fixation and reached its peak during the fixation epoch (permutation test for EARLY FIX, $p < 0.01$). The population activity in non-preferred depths and directions, instead, slightly decreased instantly after fixation onset, suggesting the presence of an inhibitory input upon these cells. The population discharge in preferred depths and directions conditions declined after the end of the fixation epoch and reached the non-preferred activity levels well before the onset of arm movement, which was maintained during action execution (LATE FIX, REACH; permutation test, $p > 0.05$).

In the Reach cells (Fig. 6c, middle row), the population responses for the preferred and non-preferred depths showed no significant changes during the fixation epoch, and the two curves progressively diverged during the movement preparation (LATE FIX, permutation test, $p < 0.01$). In the preferred condition, the curves started to increase before the onset of the arm movement and peaked just after arm movement onset. Inhibition of population activity was also observed in depth- and direction-modulated cells during the execution of non-preferred arm movements.

Fix-Reach neurons (Fig. 6c, bottom panels) showed a pattern of population responses that combined those of Fix and Reach cells. The population activity for preferred and non-preferred conditions clearly diverged immediately after fixation onset and remained separated during all other epochs considered (permutation test, $p < 0.01$ in EARLY FIX, LATE FIX, REACH, $p < 0.05$ in HOLD) for both depth and direction. Two peaks of activity, one ~ 300 ms after fixation onset and the other just after reaching onset, were observed. Interestingly, the activity in non-preferred conditions decreased both during EARLY FIX (see also Fix cells, top row of Fig. 6c) and REACH, and the selectivity dropped in between the EARLY FIX and the LATE FIX, especially for Fix-Reach cells only modulated by direction. This loss of selectivity is likely to reflect weak tonic fixation signals in PE, and this is corroborated by the results of the 2-way ANOVA (Fig. 4), where the proportion of neurons modulated during EARLY FIX is significantly lower than in the other epochs (two-proportion z-test, $p < 0.01$). In sum, depth and directionally tuned neurons showed similar temporal evolution in both Fix and Reach cell classes. Related to this finding, it should be clarified that the fact that the directionally tuned activity peaked early in the trial and depth tuned activity peaked later was due to the different proportions of depth and direction-tuned cells across the task, and not to the discharge pattern of each class.

To address how the neuronal activity of the entire recorded population of medial PE neurons changes during the reach task, independent of any preselection of neuronal subclasses (as in Fig. 6c), we computed the cumulative SDFs of PE cells considering the entire population of recorded neurons ($N = 176$), even those not modulated by depth and direction during any of the task epochs (2-way ANOVA, $p > 0.05$). The strongest response was classified as the preferred one, and the weakest as the non-preferred. As

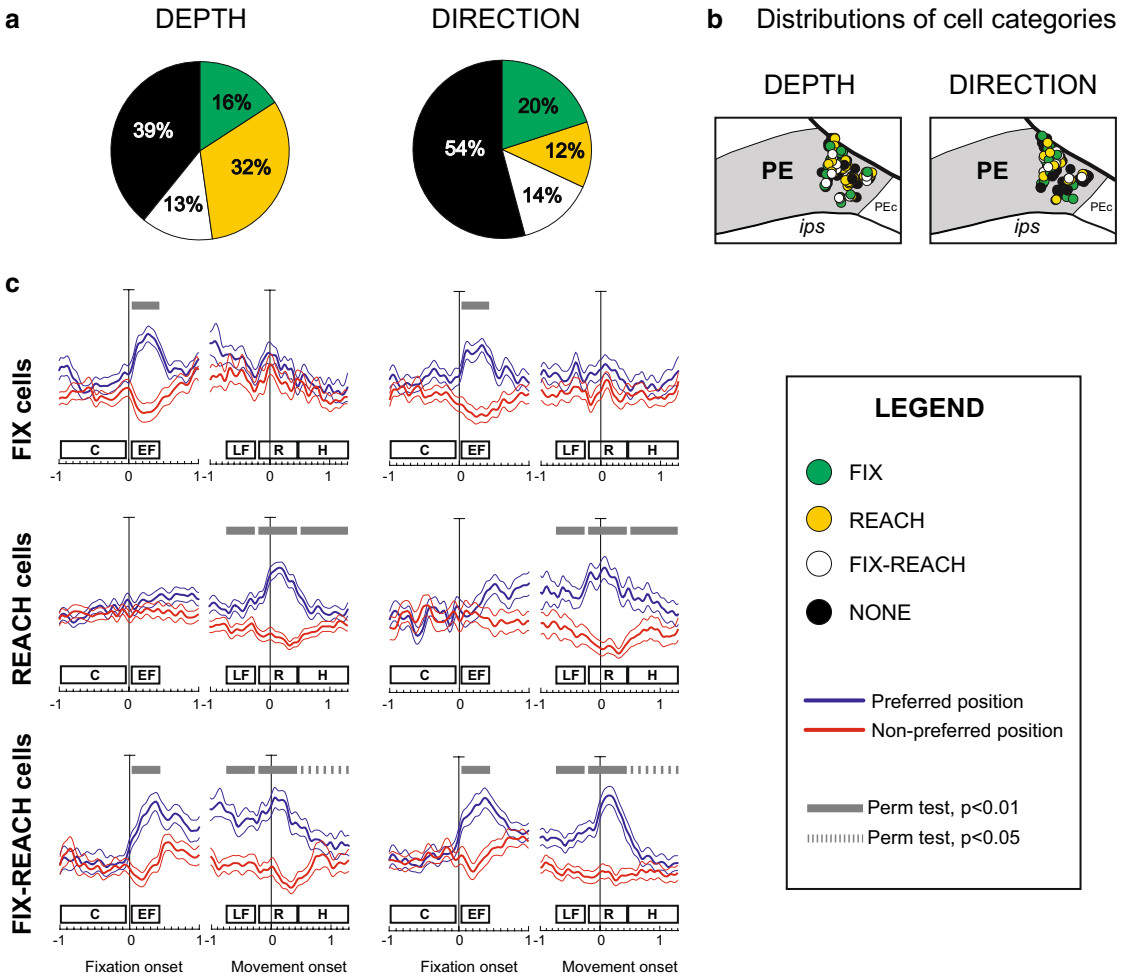

Fig. 6 Main cell categories in PE, their anatomical distribution and their population discharge. **a** Percentage of neurons modulated by depth (left) and direction (right) in both EARLY FIX and REACH epochs (Fix-Reach cells; white), in EARLY FIX but not in REACH (Fix cells; green), and vice versa (Reach cells; yellow) or in none of them (black). **b** Two dorsal views of PE (see Fig. 2) representing the distributions of the different categories of cells modulated by depth (left) and direction (right). Each circle represents one cell. **c** Population activity of the main categories of PE cells, represented as average normalized SDFs of Fix (top), Reach (middle), and Fix-Reach cells (bottom) modulated by depth (left) and direction (right), aligned twice (vertical lines) at the fixation onset and at the movement onset. For each cell category and type of modulation, the average SDFs for the preferred (blue) and non-preferred positions (red) are plotted. Thin lines in SDF represent the standard error of the mean. Scale bar in all SDF plots: 100% of normalized activity. Lines above epoch rectangles indicate where the permutation test was significant (dashed lines, $p < 0.05$; solid lines, $p < 0.01$). Other conventions as in Figs. 2 and 4

shown in Fig. 7, the SDFs of the preferred (blue line) and non-preferred (red line) conditions significantly separated immediately after fixation onset (epoch EF) and became particularly prominent during the movement preparation and execution phases of the task (epochs LF and R, permutation test, $p < 0.01$). A clear peak in activity can be observed in the preferred condition, immediately after movement onset, whereas activity in the non-preferred condition decreased particularly during the execution phase (epoch R). The shape of the curves and their time courses resemble the population response of the Reach cells (Fig. 6c, middle panels), thus strongly suggesting that, also at population level, PE neurons process more prominently skeletomotor than visuospatial signals.

Overall, neural activity remained stable and low after the EARLY FIX epoch (middle panels of Fig. 6c and Fig. 7), suggesting that eye position does not have a strong modulating influence in PE.

To test whether the target onset could possibly lead to short-latency visual responses, we also calculated the SDFs aligned to the target onset. There was no clear increase of discharge after target onset, thus confirming a lack of visual responses in area PE that has been reported in literature (Mountcastle et al. 1975; Maimon and Assad 2006; Cui and Andersen 2011; Shi et al. 2013).

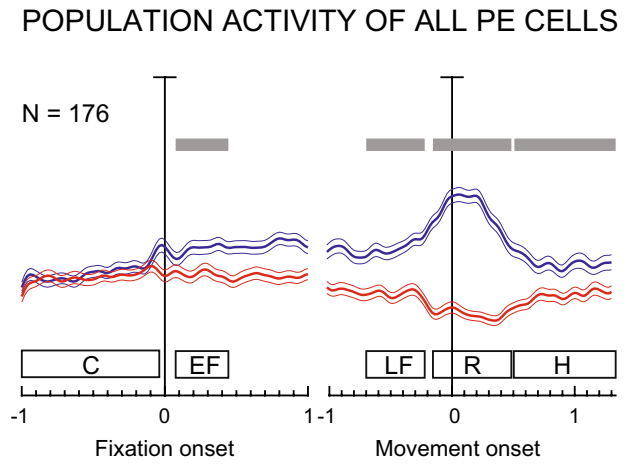

Fig. 7 Average normalized SDF of the whole population of recorded PE neurons ($N=176$). Permutation test between preferred and non-preferred position in EARLY FIX, LATE FIX, REACH, HOLD, $p<0.01$. All conventions are as in Fig. 6c

Sensory properties in the recorded region

To characterize the sensory properties of the recorded medial PE sector, we qualitatively examined the visual and somatosensory responses of a separate group of PE cells recorded in the same region as the cells tested with the reaching task, by using two additional tests (Visual and Passive Somatosensory stimulations, see "Materials and methods"). The results of these sensory stimulations showed that the part of PE we studied is strongly affected by somatosensory inputs but poorly by visual inputs (Fig. 8a, b), similarly to what has been found by other studies in the lateral part of PE (see Seelke et al. 2012 for refs). Eighty-seven percent of neurons ($N=53/61$) were responsive to somatic stimulations (see "Materials and methods"), whereas only 2% of neurons ($N=1/60$) were sensitive to visual stimulations.

Regarding the type of somatosensory input, we found that the majority of cells modulated by passive somatosensory stimulations responded to joint rotations (89%, $N=47/53$), whereas only 4% responded to tactile stimulation and 7% to both joint rotations and tactile stimulation (Fig. 8c). The distribution of somatosensory receptive fields did not match the somatotopy reported for the nearby Brodmann's area 2 (see Fig. 1). We did not find a mere representation of the lower limb, as expected if medial PE had a somatotopy complementary to the upper limb representation in lateral PE. Instead, we found intermingled lower and upper limb representations, together with sporadic representations of the trunk (Fig. 8f). Joint-sensitive cells were mostly activated by input coming from the arms (23%) and the legs (26%).

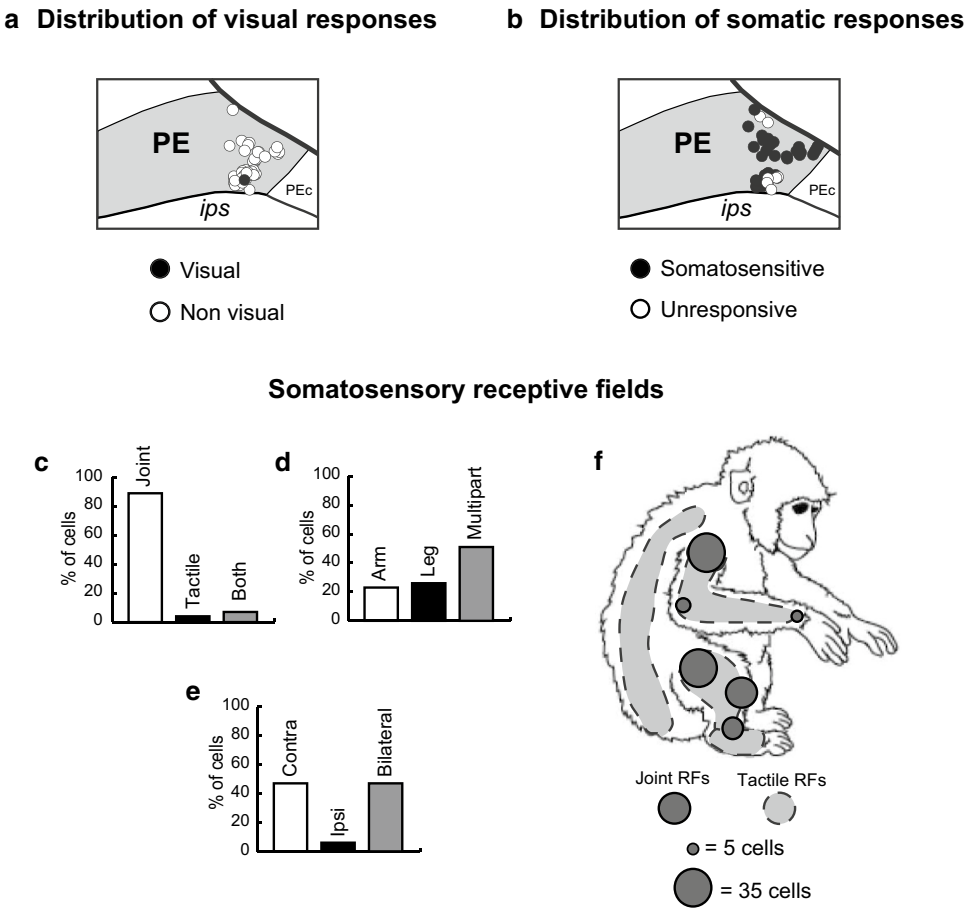

Fig. 8 Sensory properties of PE cells. Anatomical distributions of the neurons showing visual **(a)** and somatic **(b)** responses. **a** 'Visual' cells are shown in black, 'Non-visual' cells in white. **b** Somatosensitive cells are shown in black, unresponsive cells in white. **c** Incidence of cells responsive to joint, tactile or joint + tactile (Both) stimulations. **d** Incidence of cells modulated by stimulations of different parts of the body. **e** Incidence of contralateral (Contra), ipsilateral (Ipsi), and Bilateral modulations. Abbreviations as in Fig. 3. **f** Locations of somatosensory receptive fields in PE: joints (circles) and tactile receptive fields (dashed lines drawn on the animal body). The size of each circle is proportional to the number of modulated units. All somatosensory receptive fields have been reported on the right side of the body

The remaining 51% of somatosensory cells were activated by input coming from multiple parts of the body (e.g. arms, legs, trunk, Fig. 8d). A high percentage of somatosensory responses (47%) were evoked by contralateral stimulation and an equal number of cells (47%) responded to stimulation of both sides (bilateral), with only 6% of cells with somatosensory receptive fields on the ipsilateral side (Fig. 8e).

Discussion

Our aim was to functionally characterize the most medial and caudal part of area PE and to examine the relative influence of depth and direction signals during a Fixation-to-Reach task in 3D. We aimed to reproduce everyday life reaching conditions, with the arm moving in different directions and depths and a natural sequence of eye–hand coordination that involves fixation of the target before the arm movement (Neggers and Bekkering 2001; Hayhoe et al. 2003). We are aware that a contribution from gaze signals to differences in activity during reach execution cannot be excluded. However, to the best of our knowledge, there is no evidence supporting a strong modulating effect of gaze position on neural activity in PE. To this regard, Ferraina et al. (2009) investigated how the vergence angle, and initial hand position influenced PE reach-related activity. They showed that a large proportion of PE neurons was influenced by changes in hand position, while the effect of binocular eye position was small (~ 10% of neurons were affected by changes in fixation distance). Moreover, looking at Fig. 6c (middle panels, population activity of Reach cells), and Fig. 7, where the entire recorded population activity is shown, it is clear that neural activity remained stable and low after fixation onset and throughout the subsequent fixation period. It started to increase only towards movement onset. These findings suggest that gaze signals have a relatively weak influence on PE neural activity during the reach phase. Gaze position modulations in PE may derive from the thalamic centromedian (CM) nucleus, that exhibits a variety of eye movement-related signals (Tanaka 2005; Kunimatsu and Tanaka 2012), even if the connections with PE are quite weak (Impieri et al. 2018). Another source of tonic eye position signals could be the nucleus prepositus hypoglossi (NHP) in the brainstem that has been characterized as an integrator of horizontal oculomotor commands (Moschovakis et al. 1996). This nucleus has been reported to send projections, via thalamus, to the nearby medial intraparietal area (MIP) of SPL (Prevosto et al. 2009). Since the reported NHP input was heavily lateralized, this could result in some form of asymmetry in the cortical coding of eye position that would not necessarily be captured by binocular version/vergence measurements. It would be interesting to check whether the monocular (contralateral) eye position associated with the three different depths could provide a better prediction of neural activity. This issue will be addressed for all SPL areas in future studies.

We show that medial PE activity was tuned by both depth and direction of reaching, but the processing of the two parameters followed a different time course as the task progressed. Direction-tuned cells were most abundant just after target fixation, outnumbering depth-tuned cells during that period. Depth tuning increased during arm movement and target holding. These findings are in agreement with behavioral studies suggesting independent processing of reach direction and extent or amplitude information (Soechting and Flanders 1989; Flanders and Soechting 1990; Gordon et al. 1994; Sainburg et al. 2002; Vindras et al. 2005; Bagesteiro et al. 2006; Van Pelt and Medendorp 2008; Crawford et al. 2011). Moreover, we found that depth and direction signals affected separate populations of medial PE cells, and that the almost continuous pattern of activity modulation in the Fix-Reach population represents an eye-/arm-related tuning that could suggest an independent encoding of depth and direction signals. Similar findings were reported in lateral PE, though with a different task configuration (Lacquaniti et al. 1995). In that study, three different workspaces were used: reaches started from the center of each workspace towards 8 different directions evenly distributed between two depth planes. Although reach amplitude along the depth axis was not varied, targets did vary in depth with respect to the body. Despite these methodological differences Lacquaniti et al. (1995) described different pools of lateral PE neurons controlling for target direction (elevation and azimuth) and distance from the shoulder. This similarity was not granted, since medial PE neighbors and is connected to PEc, an area showing convergence of depth and direction signals (Hadjidimitrakis et al. 2015, see also below), whereas lateral PE lies further away (Fig. 1) and is less strongly connected with PEc (Bakola et al. 2013). The segregated depth and direction processing observed in both PE sectors suggests that PE processes uniformly reach-related signals.

Ferraina et al. (2009) studied a sector of area PE that partially overlapped with our recording region (Fig. 1b). Despite task differences (reach targets were extrafoveal there and arm movements were made towards memorized targets that were distributed at different distances, thus leaving out direction), their analytical approach resembles the one used in the present study, thus allowing a direct comparison with our findings. Overall, their results are in line with ours, starting from the proportion of neurons showing a task-related activity (ANOVA, 77.4%). They showed that the incidence of depth-modulated neurons increased going from target presentation to movement execution, and only a small proportion among these neurons was influenced by target presentation (6.3%). A polynomial contrast analysis, used to test which model better fitted the relationship between target depth and neural

activity, revealed that 80% of depth-modulated neurons showed a significant fit for the linear model. Furthermore, they tested a subpopulation of PE neurons with the same reach-in-depth paradigm, but varied the relative position in depth of both reach targets and fixation point across different trials and found that the effect of binocular eye position variation was negligible. Also Brunamonti et al. (2016) and Bremner and Andersen (2012) recording sites partly covered our recording region but, as they investigated the reference frames of reaching responses, a direct comparison of our results with these two latter studies is not possible. In the present study reaches were always performed towards foveated targets and started from the same initial hand position, so the frames of reference of reach-related activity could not be determined. We acknowledge that the effects of depth and direction we observed could also reflect vector coding in addition to positional coding, however, the issue of the reference frames was beyond the scope of the present work.

In our sensory mapping experiment, the majority of our medial PE recording sites showed somatosensory sensitivity, with many cells responding to stimulations of both upper and lower limbs, suggesting a role in arm-leg coordination and postural control. This is most likely because the medial part of PE studied here lies even further medial than that studied by Padberg and coworkers (2019). Interestingly, the majority of our PE neurons tuned by depth showed a bias for far space during both movement execution and target holding (Fig. 5a, b). In addition, arm-leg coordination could be more important for postural adjustments when the monkey reaches and holds the farthest targets. The integration of sensory inputs from both effectors could be reflected in increased levels of activity and/or a larger pool of responsive neurons.

Comparison of PE with SPL areas PEc and V6A

We used the same experimental paradigm in our previous V6A and PEc studies (Hadjidimitrakis et al. 2014a, 2015), enabling a direct comparison of the three SPL areas (Fig. 9). Depth processing occurred mainly during and after movement execution in both PE and PEc, whereas in V6A it was evident during all phases of the task. The number of PE cells coding for direction during the initial target fixation period

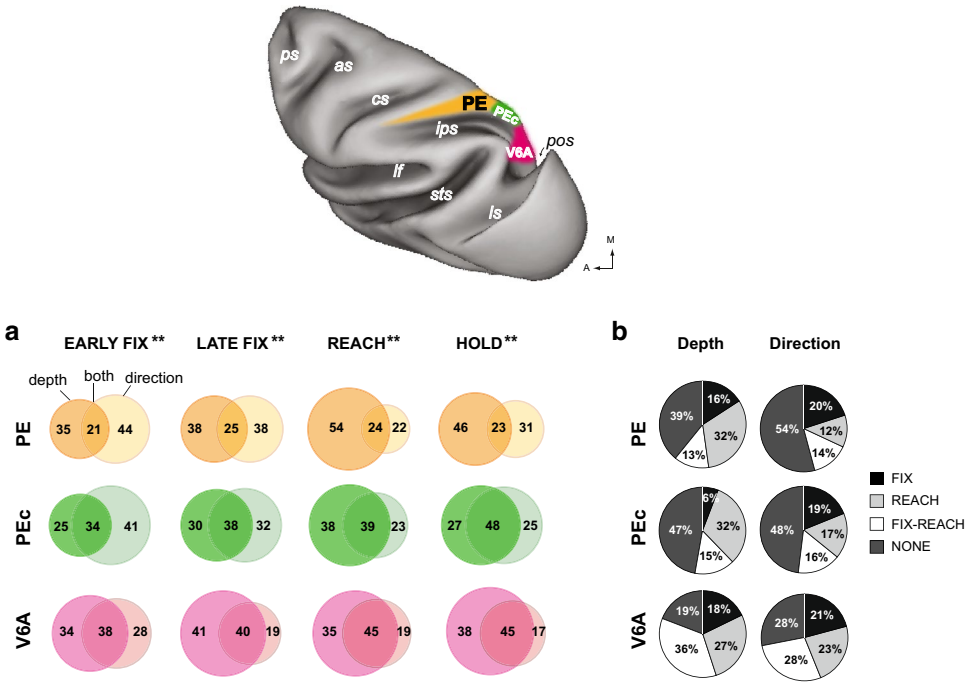

Fig. 9 Depth and direction tuning along the reaching task (**a**) and in subpopulations of cells (**b**) in 3 SPL areas. **a** Percentage of cells in PE, PEc and V6A with tuning for depth only (left set), direction only (right set), and both signals (intersection) during different task epochs (2-way ANOVA, $p<0.05$). Note that epochs EARLY FIX and LATE FIX in this study correspond to epochs FIX and DELAY in Hadjidimitrakis et al. (2014a) and (2015). Double asterisks indicate significant difference between the three areas (V6A: pink; PEc: green; PE: orange) in the coding of one or both spatial parameters in a certain epoch (Chi squared test, $p<0.01$). Data from PE: current results ($N=176$); data from V6A ($N=288$) are from Hadjidimitrakis et al. (2014a); data from PEc ($N=200$) are from Hadjidimitrakis et al. (2015), but recalculated with $p<0.05$ to standardize the criteria used in the other areas. Abbreviations as in Fig. 2, conventions as in Fig. 5a. **b** Percentage of Fix, Reach, and Fix-Reach neurons in PE, PEc, and V6A with modulations by depth (left panels) and direction (right panels). Conventions as in Figs. 6a and 9a

was higher compared to the subsequent phases, exactly as in V6A and PEc. At a population level there was a persistent higher activity for the preferred direction/depth during EARLY and LATE FIX in V6A and PEc (Hadjidimitrakis et al. 2014a, 2015) compared to PE (Fig. 6c), and the selectivity was maintained in between the two epochs, possibly reflecting a more sustained influence of fixation. The most notable trend among the three areas regards the rostro-caudal convergence of depth and direction signals on single cells: the two signals are mostly coded separately in PE (see 'both' in Fig. 9), whereas they showed a medium to high degree of convergence in PEc and V6A, respectively. This may reflect the neural correlates of the visuomotor tranformation occurring from V6A, where cells tuned for direction and depth code the target location in 3D space, to the somatomotor cortex, where PEc and PE cells tuned only for depth or for direction gradually transform target coordinates from extrinsic to intrinsic ones. Moreover, it should be noted that PEc and V6A show convergence of somatic and visual inputs related to reaching/grasping (Breveglieri et al. 2008; Gamberini et al. 2017), whereas area PE mainly hosts somatic signals. Conceivably, these different visuo-somatic properties influence the processing of depth and direction signals too. In this regard, psychophysical evidence suggests that proprioception is more linked with movement depth, whereas vision is more related to direction processing (van Beers et al. 2002, 2004). We can suggest that in PE, the target location is re-specified in terms of the shoulder and elbow joint angles, suggesting that distance primarily pertains to elbow joint extension, and direction to shoulder angle. The activity of putative elbow and shoulder processing units in PE might represent the current joint angles, the intended joint angles (i.e. the target), or a vector linking the two. Whilst activity during early fixation can plausibly be interpreted as representing target-position, activity during reach might represent proprioceptive reafference, or (a copy of) a motor command, as suggested by the early onset of reaching activity that we have found here. The command might either specify the target joint angles, or the error vectors from the current positions. Error vectors are likely being represented in PE, as suggested by the absence of preference for intermediate positions and by the predominance of 'far' tuning (Fig. 5a).

Our visual and somatosensory mapping of medial PE is in line with data from lateral PE showing strong somatosensory (Sakata et al. 1973; Bakola et al. 2013), but weak visual (Mountcastle et al. 1975; Seelke et al. 2012) responses. Compared to PE, PEc and V6A contain much more visual cells (PEc: ~ 50%, Breveglieri et al. 2008; V6A: ~ 65%, Galletti et al. 1996, 1999) but less somatosensory neurons (PEc: ~ 50%, Breveglieri et al. 2006, V6A: ~ 30%, Breveglieri et al. 2002) (see Gamberini et al. 2017).

In both PE and PEc, depth strongly modulated neural activity during and after arm movement. In V6A, instead, depth influence was quite strong long before movement onset. The increase of depth relative to direction signals during task execution that we have found likely suggests a somatomotor rather than visual processing occurring in PE, whereas a visual rather than somatosensory processing is typifying V6A. In the same vein of functional comparison, we found that the Fix, Reach, and Fix-Reach cells in each of the 3 SPL areas showed a different evolution of depth to direction tuning during the course of the trial (see Fig. 9b). When calculating the ratio of Fix:Reach cells, we found a steady increase of directional modulations going from area V6A to PE (0.96, 1.06, 1.31, V6A-PEc-PE). The comparable ratios for depth modulated neurons showed instead a discontinous trend (0.86, 0.45, 0.64, V6A-PEc-PE), best summarised by computing a ratio of ratios (i.e. Fix:Reach (direction)/Fix:Reach (depth); 1.12, 2.37, 2.03, from V6A to PE). This finding suggests that instead of a smooth gradient there is a rather abrupt increase in the gain of the relative prominence of depth over direction tuning during the course of the trial going from V6A to PEc/PE.

The spatial encoding during arm movements to visual targets has been extensively studied in several SPL areas and accumulated evidence suggests some degree of functional heterogeneity (e.g. Kalaska et al. 1990; Batista et al. 1999; Buneo et al. 2002; Ferraina et al. 2009; Chen et al. 2009; Chang and Snyder 2010; McGuire and Sabes 2011; Cui and Andersen 2011). The most notable trend regards the reference frames employed by each area to encode the target: caudal SPL areas like V6A, MIP, and PEc represent targets in eye-centered, body-centered or mixed eye(body)/hand reference frames (Batista et al. 1999; Chang and Snyder 2010; Hadjidimitrakis et al. 2014b, 2017; Bosco et al. 2016; Piserchia et al. 2017), whereas rostral SPL areas like PE and PEip use predominantly hand-centered coding (Buneo et al. 2002; Ferraina et al. 2009; McGuire and Sabes 2011; Bremner and Andersen 2012, 2014). Our studies have revealed another SPL trend, i.e. the gradual convergence on single neurons of depth and direction signals going from PE in the exposed surface of SPL cortex to V6A. We hypothesize that a similar trend may be present also within the medial bank of the intraparietal sulcus, with MIP and PEip showing mostly combined and separate depth and direction processing, respectively.

Comparison with frontal cortex

Previous studies in PEc (Hadjidimitrakis et al. 2015) and V6A (Hadjidimitrakis et al. 2014a) find a remarkable parallel, despite task differences, with the dorsal premotor cortex (PMd, Messier and Kalaska 2000): e.g. a combined tuning for depth and direction, and their increase in convergence with task progress. Area PE shows instead a considerable degree of separation between depth and direction signals,

which is maintained throughout the task (present results, Lacquaniti et al. 1995).

But how far the SPL functional trend is reflected in the frontal cortex? When we sought for analogous processing of depth and direction signals towards primary motor cortex, we found that this region shares with medial PE the predominance of depth effect during reach execution. Naselaris et al. (2006) examined the distribution of a large number of preferred arm movement directions in M1 during reaching movements in 3D space and showed an enhanced representation for reaching directions aligned with the depth axis and a specialization in motor control for reaches in depth. This functional pattern parallels the organisation of parieto-frontal connectivity, which shows a rough symmetry around the central sulcus (more caudal SPL areas having a more rostral focus in PMd, e.g. V6Av with F7, V6Ad with rostral F2, PEc with caudal F2 and PE with S1 and M1; Shipp et al. 1998; Gamberini et al. 2009; Bakola et al. 2010, 2013; Passarelli et al. 2011). The separation of elbow and shoulder loci in the motor map of M1 also suggests the divergence of depth and direction signals from unified in PMd to separate in M1.

Comparison with the human brain

Is there a similar processing scheme for reach direction and depth in monkeys and humans? In both species, SPL is involved in sensory-motor integration (see Grefkes and Fink 2005; Culham et al. 2006), and reach-related signals have been found in several human SPL regions (Connolly et al. 2003; Hagler et al. 2007; Filimon et al. 2009; Gallivan et al. 2009; Cavina-Pratesi et al. 2010), including human V6A (Pitzalis et al. 2013; Tosoni et al. 2015). While many studies reported SPL activations for reaching or pointing performed in different directions, only a few studies report SPL activations for reaching performed at different depths. Martin et al. (2015), showed that a large swath of PPC was activated during reaching towards peripheral versus central targets. Such direction selective signals were present in areas V6A, 7A, and the medial and posterior IPS. However, using fMRI adaptation as a proxy to measure tuning curves, Fabbri et al. (2010) revealed a more restricted region within the SPL (medial to the IPS and anterior to the parieto-occipital sulcus) showing a high degree of directional selectivity. Regarding the substrates of combined depth and direction processing, Fabbri et al. (2012) reported that, going from parietal to frontal areas, the processing of distance and direction information is more segregated. Furhermore, Cavina-Pratesi et al. (2010) described differential fMRI activity for near and far reaches in anterior and posterior sectors of the superior parieto-occipital cortex. This finding calls for comparative fMRI experiments (Vanduffel et al. 2014), whereby adaptation paradigms or multi-voxel pattern analyses are used, which enable direct comparisons of single selectivity for reach direction and depth with fMRI data from both humans and monkeys.

Conclusions

This study reports that in medial PE depth and direction signals for reaching are partially processed by two distinct neuronal subpopulations. Moreover, this cortical sector integrates somatic input from both upper and lower limbs, but it does not receive visual input. Combined with our previous studies, present findings highlight the functional heterogeneity in SPL, with PE strongly influenced by somatosensory input during reaching performance and predominantly processing depth.

Acknowledgements We thank Dr Michela Gamberini for help with figure preparation, and for the anatomical reconstructions together with Dr Lauretta Passarelli; Massimo Verdosci and Francesco Campisi for technical assistance.

Funding This work was supported by EU FP7-IST-217077-EYESHOTS, by H2020-MSCA-734227 – PLATYPUS, by National Health and Medical Research Council Grant APP1082144 (Australia), by Ministero dell'Università e della Ricerca (Italy, FIRB2013 prot. RBFR132BKP), Fonds Wetenschappelijk Onderzoek-Vlaanderen: G.0007.12N Odysseus, and European Union's Horizon 2020 Framework Programme for Research and Innovation under Grant Agreement No 785907 (Human Brain Project SGA2).

Compliance with ethical standards

Conflict of interest The authors declare that they have no conflict of interest.

Ethical approval All applicable international, national, and institutional guidelines for the care and use of animals were followed. All procedures performed in this study were in accordance with the ethical standards of the University of Bologna. The study was performed in accordance with the guidelines of EU Directives (86/609/EEC; 2010/63/EU) and Italian national laws (D.L. 116-92, D.L. 26-2014) on the protection of animals used for scientific purposes. Protocols were approved by the Animal-Welfare Body of the University of Bologna.

References

Andersen RA, Cui H (2009) Intention, action planning, and decision making in parietal-frontal circuits. Neuron 63:568–583. https://doi.org/10.1016/j.neuron.2009.08.028

Andersen RA, Andersen KN, Hwang EJ, Hauschild M (2014) Optic ataxia: from balint's syndrome to the parietal reach region. Neuron 81:967–983. https://doi.org/10.1016/j.neuron.2014.02.025

Ashe J, Georgopoulos AP (1994) Movement parameters and neural activity in motor cortex and area 5. Cereb Cortex 4:590–600

Bagesteiro LB, Sarlegna FR, Sainburg RL (2006) Differential influence of vision and proprioception on control of movement distance.

Exp Brain Res 171:358–370. https://doi.org/10.1007/s00221-005-0272-y
Bakola S, Gamberini M, Passarelli L et al (2010) Cortical connections of parietal field PEc in the macaque: linking vision and somatic sensation for the control of limb action. Cereb Cortex 20:2592–2604. https://doi.org/10.1093/cercor/bhq007
Bakola S, Passarelli L, Gamberini M et al (2013) Cortical connectivity suggests a role in limb coordination for macaque area PE of the superior parietal cortex. J Neurosci 33:6648–6658. https://doi.org/10.1523/JNEUROSCI.4685-12.2013
Batista AP, Buneo CA, Snyder LH, Andersen RA (1999) Reach plans in eye-centered coordinates. Science 285:257–260
Bosco A, Breveglieri R, Hadjidimitrakis K et al (2016) Reference frames for reaching when decoupling eye and target position in depth and direction. Sci Rep 6:21646. https://doi.org/10.1038/srep21646
Bremner LR, Andersen RA (2012) Coding of the reach vector in parietal area 5d. Neuron 75:342–351. https://doi.org/10.1016/j.neuron.2012.03.041
Bremner LR, Andersen RA (2014) Temporal analysis of reference frames in parietal cortex area 5d during reach planning. J Neurosci 34:5273–5284. https://doi.org/10.1523/JNEUROSCI.2068-13.2014
Breveglieri R, Kutz DDFD, Fattori P et al (2002) Somatosensory cells in the parieto-occipital area V6A of the macaque. NeuroReport 13:2113–2116. https://doi.org/10.1097/00001756-200211150-00024
Breveglieri R, Galletti C, Gamberini M et al (2006) Somatosensory cells in area PEc of macaque posterior parietal cortex. J Neurosci 26:3679–3684. https://doi.org/10.1523/JNEUROSCI.4637-05.2006
Breveglieri R, Galletti C, Monaco S, Fattori P (2008) Visual, somatosensory, and bimodal activities in the macaque parietal area PEc. Cereb Cortex 18:806–816. https://doi.org/10.1093/cercor/bhm127
Breveglieri R, Galletti C, Dal Bò G et al (2014) Multiple aspects of neural activity during reaching preparation in the medial posterior parietal area V6A. J Cogn Neurosci 26:878–895. https://doi.org/10.1162/jocn_a_00510
Brodmann K (1909) Vergleichende lokalisationslehre der Grohirnrinde Leipzig, Barth, Germany
Brunamonti E, Genovesio A, Pani P et al (2016) Reaching-related neurons in superior parietal area 5: influence of the target visibility. J Cogn Neurosci 28:1828–1837. https://doi.org/10.1162/jocn_a_01004
Buneo CA, Jarvis MR, Batista AP, Andersen RA (2002) Direct visuomotor transformations for reaching. Nature 416:632–636. https://doi.org/10.1038/416632a
Burbaud P, Doegle C, Gross C, Bioulac B (1991) A quantitative study of neuronal discharge in areas 5, 2, and 4 of the monkey during fast arm movements. J Neurophysiol 66:429–443
Cavina-Pratesi C, Monaco S, Fattori P et al (2010) Functional magnetic resonance imaging reveals the neural substrates of arm transport and grip formation in reach-to-grasp actions in humans. J Neurosci 30:10306–10323. https://doi.org/10.1523/JNEUROSCI.2023-10.2010
Chang SWC, Snyder LH (2010) Idiosyncratic and systematic aspects of spatial representations in the macaque parietal cortex. Proc Natl Acad Sci U S A 107:7951–7956. https://doi.org/10.1073/pnas.0913209107
Chen J, Reitzen SD, Kohlenstein JB, Gardner EP (2009) Neural representation of hand kinematics during prehension in posterior parietal cortex of the macaque monkey. J Neurophysiol 102:3310–3328. https://doi.org/10.1152/jn.90942.2008
Colby CL, Duhamel JR (1991) Heterogeneity of extrastriate visual areas and multiple parietal areas in the macaque monkey. Neuropsychologia 29:517–537
Connolly JD, Andersen RA, Goodale MA (2003) FMRI evidence for a "parietal reach region" in the human brain. Exp Brain Res 153:140–145. https://doi.org/10.1007/s00221-003-1587-1
Crawford JD, Henriques DYP, Medendorp WP (2011) Three-dimensional transformations for goal-directed action. Annu Rev Neurosci 34:309–331. https://doi.org/10.1146/annurev-neuro-061010-113749
Cui H, Andersen RA (2011) Different representations of potential and selected motor plans by distinct parietal areas. J Neurosci 31:18130–18136. https://doi.org/10.1523/JNEUROSCI.6247-10.2011
Culham JC, Cavina-Pratesi C, Singhal A (2006) The role of parietal cortex in visuomotor control: what have we learned from neuroimaging? Neuropsychologia 44:2668–2684. https://doi.org/10.1016/j.neuropsychologia.2005.11.003
Duffy FH, Burchfiel JL (1971) Somatosensory system: organizational hierarchy from single units in monkey area 5. Science 172:273–275
Fabbri S, Caramazza A, Lingnau A (2010) Tuning curves for movement direction in the human visuomotor system. J Neurosci 30:13488–13498. https://doi.org/10.1523/JNEUROSCI.2571-10.2010
Fabbri S, Caramazza A, Lingnau A (2012) Distributed sensitivity for movement amplitude in directionally tuned neuronal populations. J Neurophysiol 107:1845–1856. https://doi.org/10.1152/jn.00435.2011
Ferraina S, Bianchi L (1994) Posterior parietal cortex: functional properties of neurons in area 5 during an instructed-delay reaching task within different parts of space. Exp Brain Res 99:175–178
Ferraina S, Brunamonti E, Giusti MA et al (2009) Reaching in depth: hand position dominates over binocular eye position in the rostral superior parietal lobule. J Neurosci 29:11461–11470. https://doi.org/10.1523/JNEUROSCI.1305-09.2009
Filimon F, Nelson JD, Huang R-S, Sereno MI (2009) Multiple parietal reach regions in humans: cortical representations for visual and proprioceptive feedback during on-line reaching. J Neurosci 29:2961–2971. https://doi.org/10.1523/JNEUROSCI.3211-08.2009
Flanders M, Soechting JF (1990) Arm muscle activation for static forces in three-dimensional space. J Neurophysiol 64:1818–1837
Fluet M-C, Baumann MA, Scherberger H (2010) Context-specific grasp movement representation in macaque ventral premotor cortex. J Neurosci 30:15175–15184. https://doi.org/10.1523/JNEUROSCI.3343-10.2010
Galletti C, Battaglini PP, Fattori P (1995) Eye position influence on the parieto-occipital area PO (V6) of the macaque monkey. Eur J Neurosci 7:2486–2501. https://doi.org/10.1111/j.1460-9568.1995.tb01047.x
Galletti C, Fattori P, Battaglini PP et al (1996) Functional demarcation of a border between areas V6 and V6A in the superior parietal gyrus of the macaque monkey. Eur J Neurosci 8:30–52. https://doi.org/10.1111/j.1460-9568.1996.tb01165.x
Galletti C, Fattori P, Kutz DF, Gamberini M (1999) Brain location and visual topography of cortical area V6A in the macaque monkey. Eur J Neurosci 11:575–582. https://doi.org/10.1046/j.1460-9568.1999.00467.x
Gallivan JP, Cavina-Pratesi C, Culham JC (2009) Is that within reach? fMRI reveals that the human superior parieto-occipital cortex encodes objects reachable by the hand. J Neurosci 29:4381–4391. https://doi.org/10.1523/JNEUROSCI.0377-09.2009
Gamberini M, Passarelli L, Fattori P et al (2009) Cortical connections of the visuomotor parietooccipital area V6Ad of the macaque

monkey. J Comp Neurol 513:622–642. https://doi.org/10.1002/cne.21980
Gamberini M, Galletti C, Bosco A et al (2011) Is the medial posterior parietal area V6A a single functional area? J Neurosci 31:5145–5157. https://doi.org/10.1523/JNEUROSCI.5489-10.2011
Gamberini M, Dal Bò G, Breveglieri R et al (2017) Sensory properties of the caudal aspect of the macaque's superior parietal lobule. Brain Struct Funct. https://doi.org/10.1007/s00429-017-1593-x
Gardner EP (2017) Neural pathways for cognitive command and control of hand movements. Proc Natl Acad Sci 114:4048–4050. https://doi.org/10.1073/pnas.1702746114
Gardner EP, Babu KS, Reitzen SD et al (2007) Neurophysiology of prehension. I. Posterior parietal cortex and object-oriented hand behaviors. J Neurophysiol 97:387–406. https://doi.org/10.1152/jn.00558.2006
Gordon J, Ghilardi MF, Ghez C (1994) Accuracy of planar reaching movements. I. Independence of direction and extent variability. Exp Brain Res 99:97–111
Grefkes C, Fink GR (2005) REVIEW: the functional organization of the intraparietal sulcus in humans and monkeys. J Anat 207:3–17. https://doi.org/10.1111/j.1469-7580.2005.00426.x
Hadjidimitrakis K, Breveglieri R, Placenti G et al (2011) Fix your eyes in the space you could reach: neurons in the macaque medial parietal cortex prefer gaze positions in peripersonal space. PLoS One 6:e23335. https://doi.org/10.1371/journal.pone.0023335
Hadjidimitrakis K, Breveglieri R, Bosco A, Fattori P (2012) Three-dimensional eye position signals shape both peripersonal space and arm movement activity in the medial posterior parietal cortex. Front Integr Neurosci 6:37. https://doi.org/10.3389/fnint.2012.00037
Hadjidimitrakis K, Bertozzi F, Breveglieri R et al (2014a) Common neural substrate for processing depth and direction signals for reaching in the monkey medial posterior parietal cortex. Cereb Cortex 24:1645–1657. https://doi.org/10.1093/cercor/bht021
Hadjidimitrakis K, Bertozzi F, Breveglieri R et al (2014b) Body-centered, mixed, but not hand-centered coding of visual targets in the medial posterior parietal cortex during reaches in 3D space. Cereb Cortex 24:3209–3220. https://doi.org/10.1093/cercor/bht181
Hadjidimitrakis K, Dal Bò G, Breveglieri R et al (2015) Overlapping representations for reach depth and direction in caudal superior parietal lobule of macaques. J Neurophysiol 114:2340–2352. https://doi.org/10.1152/jn.00486.2015
Hadjidimitrakis K, Bertozzi F, Breveglieri R et al (2017) Temporal stability of reference frames in monkey area V6A during a reaching task in 3D space. Brain Struct Funct 222:1959–1970. https://doi.org/10.1007/s00429-016-1319-5
Hagler DJ, Riecke L, Sereno MI (2007) Parietal and superior frontal visuospatial maps activated by pointing and saccades. Neuroimage 35:1562–1577. https://doi.org/10.1016/j.neuroimage.2007.01.033
Hayhoe MM, Shrivastava A, Mruczek R, Pelz JB (2003) Visual memory and motor planning in a natural task. J Vis 3:6. https://doi.org/10.1167/3.1.6
Hinkley LB, Krubitzer LA, Nagarajan SS, Disbrow EA (2007) Sensorimotor integration in S2, PV, and parietal rostroventral areas of the human sylvian fissure. J Neurophysiol 97:1288–1297. https://doi.org/10.1152/jn.00733.2006
Impieri D, Gamberini M, Passarelli L et al (2018) Thalamo-cortical projections to the macaque superior parietal lobule areas PEc and PE. J Comp Neurol 526:1041–1056. https://doi.org/10.1002/cne.24389
Johnson PB, Ferraina S, Bianchi L, Caminiti R (1996) Cortical networks for visual reaching: physiological and anatomical organization of frontal and parietal lobe arm regions. Cereb Cortex 6:102–119
Jones EG, Coulter JD, Hendry SH (1978) Intracortical connectivity of architectonic fields in the somatic sensory, motor and parietal cortex of monkeys. J Comp Neurol 181:291–347. https://doi.org/10.1002/cne.901810206
Kalaska JF (1996) Parietal cortex area 5 and visuomotor behavior. Can J Physiol Pharmacol 74:483–498
Kalaska JF, Crammond DJ (1992) Cerebral cortical mechanisms of reaching movements. Science 255:1517–1523
Kalaska JF, Caminiti R, Georgopoulos AP (1983) Cortical mechanisms related to the direction of two-dimensional arm movements: relations in parietal area 5 and comparison with motor cortex. Exp Brain Res 51:247–260
Kalaska JF, Cohen DA, Hyde ML (1985) Role of the motor and parietal cortex in the control of visually-guided arm movements. Union Med Can 114:1006–1010
Kalaska JF, Cohen DA, Prud'homme M, Hyde ML (1990) Parietal area 5 neuronal activity encodes movement kinematics, not movement dynamics. Exp Brain Res 80:351–364
Kunimatsu J, Tanaka M (2012) Alteration of the timing of self-initiated but not reactive saccades by electrical stimulation in the supplementary eye field. Eur J Neurosci 36:3258–3268. https://doi.org/10.1111/j.1460-9568.2012.08242.x
Kutz DF, Fattori P, Gamberini M et al (2003) Early- and late-responding cells to saccadic eye movements in the cortical area V6A of macaque monkey. Exp Brain Res 149:83–95. https://doi.org/10.1007/s00221-002-1337-9
Kutz DF, Marzocchi N, Fattori P et al (2005) Real-time supervisor system based on trinary logic to control experiments with behaving animals and humans. J Neurophysiol 93:3674–3686. https://doi.org/10.1152/jn.01292.2004
Lacquaniti F, Guigon E, Bianchi L et al (1995) Representing spatial information for limb movement: role of area 5 in the monkey. Cereb Cortex 5:391–409
Li Y, Cui H (2013) Dorsal parietal area 5 encodes immediate reach in sequential arm movements. J Neurosci 33:14455–14465. https://doi.org/10.1523/JNEUROSCI.1162-13.2013
Mackay WA, Mendonça AJ, Riehle A (1994) Spatially modulated touch responses in parietal cortex. Brain Res 645:351–355. https://doi.org/10.1016/0006-8993(94)91673-X
Maimon G, Assad JA (2006) Parietal area 5 and the initiation of self-timed movements versus simple reactions. J Neurosci 26:2487–2498. https://doi.org/10.1523/JNEUROSCI.3590-05.2006
Martin JA, Karnath H-O, Himmelbach M (2015) Revisiting the cortical system for peripheral reaching at the parieto-occipital junction. Cortex 64:363–379. https://doi.org/10.1016/j.cortex.2014.11.012
Marzocchi N, Breveglieri R, Galletti C, Fattori P (2008) Reaching activity in parietal area V6A of macaque: eye influence on arm activity or retinocentric coding of reaching movements? Eur J Neurosci 27:775–789. https://doi.org/10.1111/j.1460-9568.2008.06021.x
McGuire LMM, Sabes PN (2011) Heterogeneous representations in the superior parietal lobule are common across reaches to visual and proprioceptive targets. J Neurosci 31:6661–6673. https://doi.org/10.1523/JNEUROSCI.2921-10.2011
Menzer DL, Rao NG, Bondy A et al (2014) Population interactions between parietal and primary motor cortices during reach. J Neurophysiol 112:2959–2984. https://doi.org/10.1152/jn.00851.2012
Messier J, Kalaska JF (2000) Covariation of primate dorsal premotor cell activity with direction and amplitude during a memorized-delay reaching task. J Neurophysiol 84:152–165

Moschovakis AK, Scudder CA, Highstein SM (1996) The microscopic anatomy and physiology of the mammalian saccadic system. Prog Neurobiol 50:133–254

Mountcastle VB, Lynch JC, Georgopoulos A et al (1975) Posterior parietal association cortex of the monkey: command functions for operations within extrapersonal space. J Neurophysiol 38:871–908

Nakamura K, Colby CL (2000) Visual, saccade-related, and cognitive activation of single neurons in monkey extrastriate area V3A. J Neurophysiol 84:677–692

Naselaris T, Merchant H, Amirikian B, Georgopoulos AP (2006) Large-scale organization of preferred directions in the motor cortex. I. Motor cortical hyperacuity for forward reaching. J Neurophysiol 96:3231–3236. https://doi.org/10.1152/jn.00487.2006

Neggers SF, Bekkering H (2001) Gaze anchoring to a pointing target is present during the entire pointing movement and is driven by a non-visual signal. J Neurophysiol 86:961–970

Nelissen K, Vanduffel W (2011) Grasping-related functional magnetic resonance imaging brain responses in the macaque monkey. J Neurosci 31:8220–8229. https://doi.org/10.1523/JNEUROSCI.0623-11.2011

Nelissen K, Fiave PA, Vanduffel W (2018) Decoding grasping movements from the parieto-frontal reaching circuit in the nonhuman primate. Cereb Cortex 28:1245–1259. https://doi.org/10.1093/cercor/bhx037

Padberg J, Franca JG, Cooke DF et al (2007) Parallel evolution of cortical areas involved in skilled hand use. J Neurosci 27:10106–10115. https://doi.org/10.1523/JNEUROSCI.2632-07.2007

Padberg J, Cooke DF, Cerkevich CM et al (2019) Cortical connections of area 2 and posterior parietal area 5 in macaque monkeys. J Comp Neurol 527:718–737. https://doi.org/10.1002/cne.24453

Pandya DN, Seltzer B (1982) Intrinsic connections and architectonics of posterior parietal cortex in the rhesus monkey. J Comp Neurol 204:196–210. https://doi.org/10.1002/cne.902040208

Passarelli L, Rosa MGP, Gamberini M et al (2011) Cortical connections of area V6Av in the macaque: a visual-input node to the eye/hand coordination system. J Neurosci 31:1790–1801. https://doi.org/10.1523/JNEUROSCI.4784-10.2011

Piserchia V, Breveglieri R, Hadjidimitrakis K et al (2017) Mixed body/hand reference frame for reaching in 3D space in macaque parietal area PEc. Cereb Cortex. https://doi.org/10.1093/cercor/bhw039

Pitzalis S, Sereno MI, Committeri G et al (2013) The human homologue of macaque area V6A. Neuroimage 82:517–530. https://doi.org/10.1016/j.neuroimage.2013.06.026

Pons TP, Garraghty PE, Cusick CG, Kaas JH (1985) The somatotopic organization of area 2 in macaque monkeys. J Comp Neurol 241:445–466. https://doi.org/10.1002/cne.902410405

Prevosto V, Graf W, Ugolini G (2009) Posterior parietal cortex areas MIP and LIPv receive eye position and velocity inputs via ascending preposito-thalamo-cortical pathways. Eur J Neurosci 30:1151–1161. https://doi.org/10.1111/j.1460-9568.2009.06885.x

Rathelot J-A, Dum RP, Strick PL (2017) Posterior parietal cortex contains a command apparatus for hand movements. Proc Natl Acad Sci 114:4255–4260. https://doi.org/10.1073/pnas.1608132114

Sainburg RL, Lateiner JE, Latash ML, Bagesteiro LB (2002) Effects of altering initial position on movement direction and extent. J Neurophysiol 89:401–415. https://doi.org/10.1152/jn.00243.2002

Sakata H, Takaoka Y, Kawarasaki A, Shibutani H (1973) Somatosensory properties of neurons in the superior parietal cortex (area 5) of the rhesus monkey. Brain Res 64:85–102

Scott SH, Sergio LE, Kalaska JF (1997) Reaching movements with similar hand paths but different arm orientations. II. Activity of individual cells in dorsal premotor cortex and parietal area 5. J Neurophysiol 78:2413–2426

Seelke AMH, Padberg JJ, Disbrow E et al (2012) Topographic maps within Brodmann's area 5 of macaque monkeys. Cereb Cortex 22:1834–1850. https://doi.org/10.1093/cercor/bhr257

Shi Y, Apker G, Buneo CA (2013) Multimodal representation of limb endpoint position in the posterior parietal cortex. J Neurophysiol 109:2097–2107. https://doi.org/10.1152/jn.00223.2012

Shipp S, Blanton M, Zeki S (1998) A visuo-somatomotor pathway through superior parietal cortex in the macaque monkey: cortical connections of areas V6 and V6A. Eur J Neurosci 10:3171–3193. https://doi.org/10.1046/j.1460-9568.1998.00327.x

Soechting JF, Flanders M (1989) Sensorimotor representations for pointing to targets in three-dimensional space. J Neurophysiol 62:582–594

Snyder LH, Batista AP, Andersen RA (1997) Coding of intention in the posterior parietal cortex. Nature 386:167–170

Tanaka M (2005) Involvement of the central thalamus in the control of smooth pursuit eye movements. J Neurosci 25:5866–5876. https://doi.org/10.1523/JNEUROSCI.0676-05.2005

Taoka M, Toda T, Iwamura Y (1998) Representation of the midline trunk, bilateral arms, and shoulders in the monkey postcentral somatosensory cortex. Exp Brain Res 123:315–322

Tosoni A, Pitzalis S, Committeri G et al (2015) Resting-state connectivity and functional specialization in human medial parieto-occipital cortex. Brain Struct Funct 220:3307–3321. https://doi.org/10.1007/s00429-014-0858-x

van Beers RJ, Wolpert DM, Haggard P (2002) When feeling is more important than seeing in sensorimotor adaptation. Curr Biol 12:834–837

van Beers RJ, Haggard P, Wolpert DM (2004) The role of execution noise in movement variability. J Neurophysiol 91:1050–1063. https://doi.org/10.1152/jn.00652.2003

Van Pelt S, Medendorp WP (2008) Updating target distance across eye movements in depth. J Neurophysiol 99:2281–2290. https://doi.org/10.1152/jn.01281.2007

Vanduffel W, Zhu Q, Orban GA (2014) Monkey cortex through fMRI glasses. Neuron 83:533–550. https://doi.org/10.1016/j.neuron.2014.07.015

Vindras P, Desmurget M, Viviani P (2005) Error parsing in visuomotor pointing reveals independent processing of amplitude and direction. J Neurophysiol 94:1212–1224. https://doi.org/10.1152/jn.01295.2004

Zar JH (1999) Biostatistical analysis. Prentice Hall, Englewood Cliffs